Poloxamer (PLX) Coatings Modulate Chronic Inflammation and Enhance Biocompatibility of Multichannel Microelectrode Arrays

A Thesis

Submitted to the Faculty

Of

Drexel University

By

Pradeep Kondaveeti

in partial fulfillment of the

requirements for the degree

of

Master of Science in Biomedical Engineering

May 2010

ACKNOWLEDGEMENTS

This thesis would not exist without the guidance, encouragement, and support of many individuals.

First, I would like to express my gratitude for my advisor, Dr. Karen Moxon, for her assistance and oversight of all my research endeavors for the last few years. She has given me the freedom, the resources, and the guidance to ensure my success as a researcher. Additionally, her thoughtful feedback has allowed me to become me a better engineer and will serve me in my future endeavors.

I would also like to thank my thesis committee members, Dr. Kenneth Barbee and Dr. Fred Allen for their guidance and valuable feedback they have given me in completing this work.

There are many people in the NeuroRobotics Lab who have helped complete this research work. I would like to specially thank Amrit Misra for the advice with the data analysis part and also for reviewing my overall work. I really appreciate the help of Jennifer Garcia and Dr. Jonathan Nissanov towards the completion of the histology, immunohistochemistry, and fluorescence microscopy. I would also like to thank Eric Knudsen for allowing me to use his MATLAB program and helping bring our quantification protocol into reality.

Finally, I would like to express my gratitude to all of my family members and friends for their immense support and encouragement throughout my academic career.

TABLE OF CONTENTS

LIST OF FIGURES

LIST OF TABLES

ABSTRACT

Poloxamer (PLX) Coatings to Modulate Chronic Inflammation and Enhance Biocompatibility in Multichannel Microelectrode Arrays

Pradeep Kondaveeti

Advisor: Karen Moxon, PhD

Traumatic brain injury is responsible for the loss of neural function in millions of patients across the United States every year. Neural electrodes show potential in significantly enhancing the quality of life of these patients by restoring lost communication with the body. For example, a microelectrode sensor designed for human quadriplegic patients allows them to move a cursor on the screen using single neuron activity. Long term electrode implantation in the brain, however, leads to glial scar formation, thereby limiting the functional lifetime of an electrode *in vivo*. In this thesis, we investigated the biocompatibility of ceramic based multichannel electrodes coated with Poloxamer – 188 (PLX), a bifunctionalized co-polymer that may self insert into damaged neuronal membranes and limit cellular damage. In order to do this, we first developed a method to quantify inflammatory cells around the microelectrode. Then, using immunohistochemical staining techniques, presence and expression of microglia/macrophages (ED1), astrocytes (GFAP), and intact neurons (NeuN) were observed at 2, 4, and 6 week intervals post implantation. Cells were characterized in terms of proliferation (stereological analysis) and morphology (intensity of fluorescent staining). Our results showed that PLX coated electrodes significantly reduced the presence of microglia and macrophages at 2 weeks, 4 weeks, and at 6 weeks post

implantation as evident by relative fluorescence of ED1 staining. Similarly, GFAP staining shows decreased protein expression of astrocytes at 2 week and 4 week time points. In contrast, NeuN staining revealed that PLX is associated with increased neuronal presence in the vicinity of the implant site at 2 week and 4 week time points but not at the 6 week time point. The demonstrated modulation of the immune response seen in electrodes coated with PLX coatings show promise in its future application as a mode of protecting and extending the functional lifetime of implanted neural electrodes. In the long term, we hope that implementation of a poloxamer coated microelectrode surface will lead to chronically implantable microelectrode devices capable of recording neurons for longer periods. This will enable the use of microelectrode dependent neuroprosthetics as viable alternatives to patients who have lost motor functions due to brain injury.

1. INTRODUCTION

1.1. Statement of problem

In recent years, a variety of brain machine interfaces (BMIs) have been proposed to help patients suffering from traumatic brain injury. Technologies including electroencephalography (EEG), intra-cranial microelectrodes, and intra-cortical microelectrodes have been implemented to communicate with the brain and restore lost ability for the CNS to communicate with the body [1-3]. Among these, intra cortical microelectrodes, in particular have been suggested to restore some of the voluntary motor control for severely paralyzed patients [1-3]. A prime example of such modality is the use of electrode arrays to help paralyzed patients perform computer tasks by thoughts alone [4]. While less invasive methods are available to restore motor control, they do not provide the freedom and control that recording microelectrodes provide[3]. Additionally, the recordings from these microelectrodes directly come from the brain center that used to control motor activity prior to injury, therefore increasing prosthetic control and eliminating the need for any additional training for the patients[3]. Even though the implementation of intracortical recordings hold a great promise for therapeutic treatments, the feasibility of these devices in clinical application has been hindered by poor reliability of chronic recordings from single neurons. One of the problems that hinder long term functionality of the probe is the failure of device itself [3-4]. Previous work in our lab reported that using ceramic based electrodes reduces the chance of device failure due to the additional insulation they provide during *in vivo*

recordings [5]. Our ceramic devices have the added advantage of superior mechanical properties having both higher strength and elastic modulus than the widely used silicon counterparts [5]. Even though the use of novel materials have enhanced the biocompatibility of neural probes, the dominant hypothesis for the long term failure of neural implants is due to a glial scar which is formed around the tissue, induced by the implant [6-8]. Studies show that microelectrodes elicit a biological response in the area surrounding the implant which has been suggested to cause the loss of discriminable single unit action potentials on the order of weeks [7, 9-10]. Therefore, formation of non-conductive glial scar must be minimized in order to maintain long-term *in vivo* functionality of the electrode.

1.2. Overall Objective

The primary goal of this project is to improve the long term functionality of porous silicon nanostructured ceramic microelectrodes. To achieve this, we hypothesized that administration of local anti-inflammatory drugs *via* bioactive poloxamer coatings of the neural probes will minimize the cellular and tissue response around the implanted devices. Poloxamer - 188 (PLX) is a triblock copolymer shown to promote cell viability and cell recovery once added to mechanically injured cells [11]. Serbest et al. showed that Poloxamer seals cell membranes when added to injured PC12 cells [11]. Therefore, we hypothesize that poloxamer could enhance neuronal survival and minimize glial activation following electrode injury aiding in the repair of neurons during electrode insertion. Numerous studies have reported that electrode coatings successfully improve biocompatibility and promote tissue integration with neural probes [12-13]. Many of the studies that reported the use of bioactive coatings, used line intensity profile

analysis to quantify the brain tissue reaction to implanted devices. For example, He et al. successfully quantified glial scarring in laminin coated silicon probes using the fluorescent intensity analysis program [13]. The problem however is that the intensity methods misrepresent cell counts due to variations in cell size, shape and volume. Thus, there is a need to design a process that can be used to quantify cell proliferation as well as cell hypertrophy in order to accurately assess glial scarring around the implant.

Therefore, the specific aims of this particular project are as follows:

- **To design a method to quantify the effects of microelectrode insertion on neuronal tissue**

- **To quantify the effect of poloxamer coatings on biocompatibility of microelectrodes *in vivo***

2. BACKGROUND INFORMATION

2.1. Application of microelectrodes in injury

In traumatic brain injury patients, implantable microelectrodes have been shown to have the capability to connect the brain to the external world by recording motor commands from neurons in the primary motor cortex. These commands can then be decoded these commands into electrical signals that give the ability for these patients to control lost function in limbs [14]. With the help of chronic neural recordings, amputees can interact with the environment by improving their mobility via an artificial limb or a robotic arm[14]. For example, an implantable microelectrode can be successfully designed to record single neuron activity in order for human quadriplegic patients to control a cursor on the computer screen by thoughts alone[4]. Therefore, the ability to indefinitely record single neurons with implantable electrodes holds great promise for patients with impaired motor conditions caused by stroke, spinal cord injuries, and neurodegenerative diseases.

2.2. Glial Scar formation

2.2.1. Injury repair in the Nervous System

When microelectrodes are implanted into the cortex, they tear through the nerve tissue, severing capillaries, extracellular matrix, glial and neuronal processes causing extensive damage at the site of electrode insertion [8]. This damage activates a series of foreign body responses by activating platelets, clotting factors and macrophages[15]. Following this inflammatory response, the body initiates a number of repair

mechanisms to allow for recovery from the mechanical damage[15]. In the peripheral nervous system, the damage to neurons is often repaired with the help of macrophages and Schwann cells. However, the injury to neurons in Central Nervous System (CNS) cannot be repaired due to the inability of the neurons to regenerate. This is primarily due to the continued presence of inhibitory glycoproteins in the environment. When the electrode is inserted into the CNS, the recruitment of phagocytic cells is much slower due to the presence of blood brain barrier[15]. This causes a delay in the repair mechanism and leads to the upregulation of cell adhesion molecules at the site of injury[15]. While there is significant information on the brain's response to traumatic brain injury, much less is understood about the immunological and cellular response to insertion of microelectrode and more importantly, how this response interferes with single neuron recording.

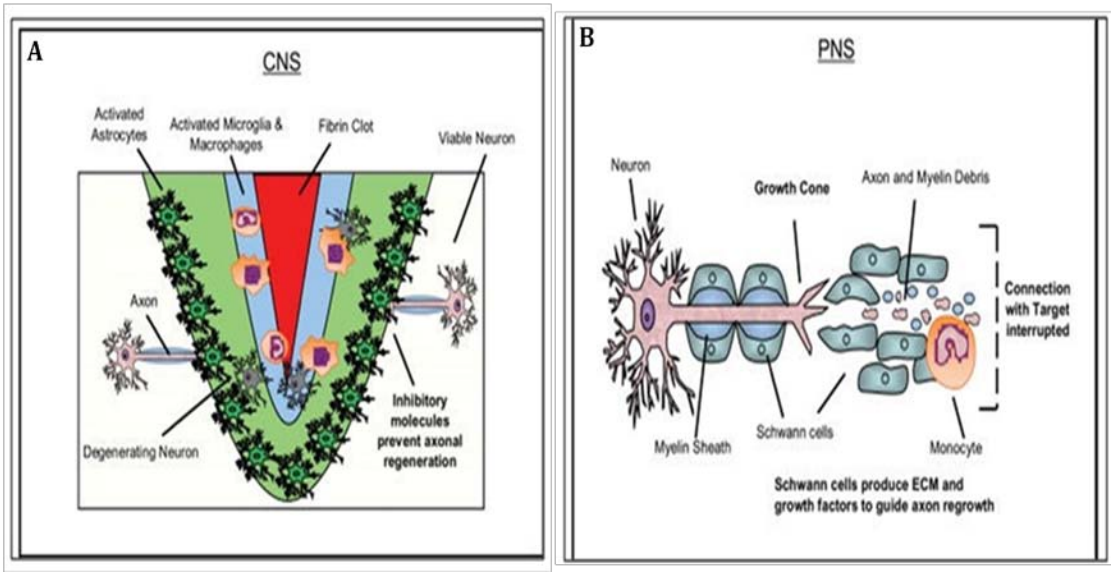

Figure 2.1 : Injury repair in the Nervous System. (A) In the CNS, phagocytic cells such as microglia and macrophages form a glial scar around the injury site. Activate astrocytes create a barrier around the damaged tissue. Production of inhibitory molecules blocks regeneration of damaged neurons. (B) After an injury in the PNS,

Schwann cells and macrophages produce ECM and growth factors and help re-innervate damaged tissue. (Figure reproduced from [16]) © CRC Press, 2008.

2.2.2. Chronic inflammation after implantation

Once a microelectrode is inserted, two types of responses are elicited in the brain [17]. First, an acute inflammatory response occurs once the microelectrode tears through the tissue during implantation and damages neuronal and glial processes [18-19]. Secondly, a chronic foreign body response arises from the long term presence of electrode tracks [18, 20]. Studies have shown that if brain is subjected to a stab wound with an electrode device, the stab wounds could not be located within 6 months of the implantation attesting the formation of a glial scar [9, 20]. In these studies, a stab wound is initiated by inserting the device, and then withdrawn, and the dura and skull are replaced over the stab site. However, in contrast to stab wounds, the long term presence of electrodes will result in a thicker glial scar around the device, effectively walling if off from healthy neural tissue[21]. Recent studies have shown that the chronic inflammatory response also persists in primates similar to rodents [22]. Griffith and Humprey observed a clear presence of chronic inflammation in monkeys with microelectrodes implanted at 3 month and 36 month time points [22] . Thus, it is important to understand the biological response to microelectrode insertion to acquire long term recordings of single neurons. In order to do this, we must first understand the different types of cells involved in the immunological response and how this response is regulated *in vivo*. Additionally, the challenges of quantifying this cellular response will be discussed through the survey of recent literature.

When an electrode is implanted, the triggered brain's reaction is a complex process involving interplay between at least three cell types *via* different cell pathways. During the glial scar formation, the main cell types involved are microglia, blood-borne macrophages, and astrocytes [16-17]. Upon electrode insertion, these cells become activated , characterized by cell proliferation and changes in cell morphology[23]. These activated cells release intracellular proteins and neurotrophic factors in to the environment, initiating a cascade of events that lead to glial proliferation and inflammation buildup [24]. This buildup of inflammatory cells pushes neurons away from the recording site and can be attributed to the failure of the implanted electrode over time [17, 24].

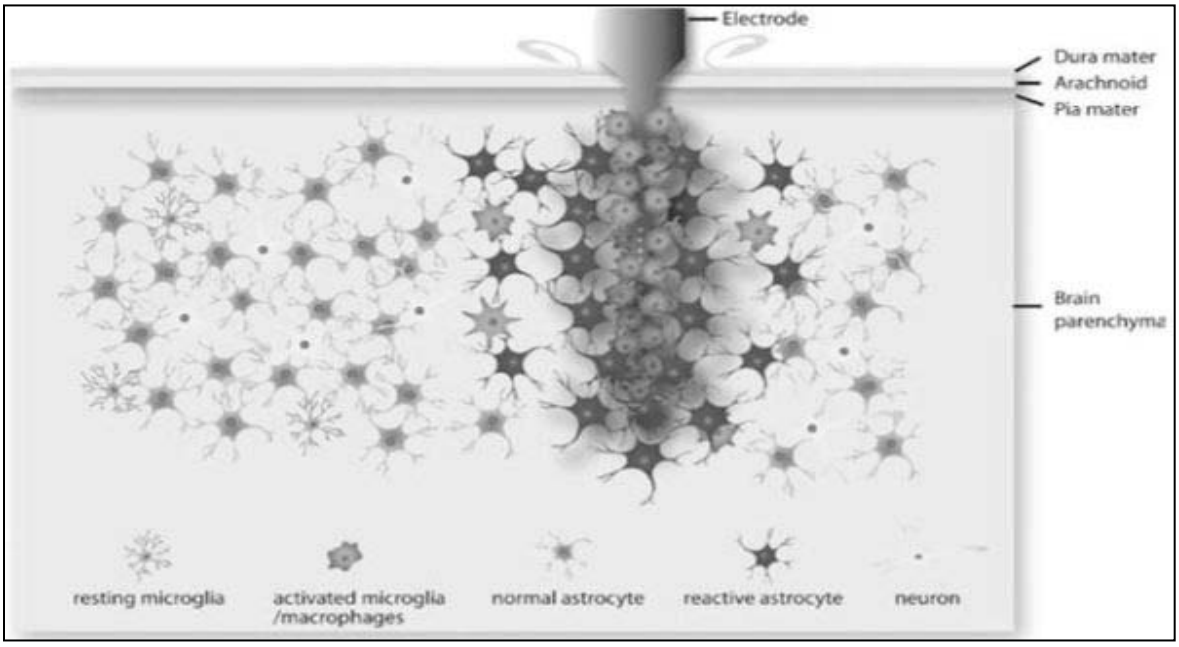

Figure 2.2: Cell types involved in response to microelectrode insertion. The above schematic shows tissue response at the cellular level following implantation. Microglia become activated characterized by amoeboid shape. Astrocytes become activated by becoming reactive, characterized by increase in size and GFAP expression. (Reproduced from [25]) © CRC Press, 2008.

2.2.3. Cellular types involved in Inflammation

After an injury to the brain, microglia are first to respond to the site and become upregulated [26]. Under healthy conditions, microglia play the role of primary defense against pathogens and are responsible for initial immune response in the CNS [27]. These cells utilize proteolytic enzymes to remove cellular debris *via* phagocytosis [26]. Within one day of electrode implantation, microglia are activated to repair the damage to blood brain barrier (BBB) [27]. Near the injury site, these glial cells exhibit changes in morphology and proliferate rapidly. It is noted that activated microglial resemble an 'amoeboid' morphology [26]. Proceeding brain injury, the activated microglia have both beneficial and detrimental effects.

Initially, activated microglia promote neuron survival by secreting neurotrophic factor and cytokines such as nerve growth factor (NGF), brain-derived neurotrophic factor (BDNF) and neurotrophin-3 (NT-3) [28-29]. These chemicals have shown to enhance axonal growth and support neuron development both *in vitro* and *in vivo [30]*. Many studies have also reported the release of interleukin-1 (IL-1), tumor necrosis factor alpha (TNF-α), and interleukin-10 (IL-10) [28-29]. Furthermore, Babcock et al. reported that microglia also play a role in the activation of astrocytes near the injury site [31]. In the beginning, microglia respond positively to injury by initiating a complex chemical signaling cascade, which leads to secretion of various neurotrophic factors that participate in injury repair.

Even though activated microglia are essential in injury repair, their long term presence can however have detrimental effects on neuronal survival due to the damage elicited from high concentrations of chemicals released in the environment. In response to injury, microglia release potent chemicals such as monocyte chemo-attractant protein (MCP-1)[28]. MCP-1 is known to recruit new microglia and macrophages, creating an inflammatory state, which walls off electrode from the healthy tissue. Additionally, cytokine production by microglia is accompanied by the production of nitric oxide (NO), which has an inhibitory effect on neuron growth [32]. Multiple studies report that the same mechanisms that help microglia to repair neural tissue, can also lead to an inflammatory state if the initial damage to the brain is severe. In the case of microelectrode insertion, activation of some microglia is beneficial to clear debris from damaged neurons and support neuronal survival by secreting neurotrophic factors. However, long term presence of electrode causes excessive damage to brain tissue leading to over proliferation of microglia and accumulation of toxic chemicals, leading to chronic inflammation and subsequent neuron death. Many researchers are trying to understand how the microglia shift from being beneficial to detrimental and working on multiple solutions to keep the microglia below that threshold level where they start creating damage to neural tissue. Thus, one of the goals of our study is to understand the role of microglia and eventually block its negative effects in order to aid in the long term success of chronically implanted microelectrodes.

Macrophages are another cell type that makes up brain's response to electrode insertion. Macrophages are not present in normal brain tissue but circulate within the vasculature [32]. During electrode insertion, blood vessels are severed, releasing

monocytes in to the neural tissue. The damage to BBB induces changes to the monocytes, leading to formation of macrophages. These newly formed macrophages morphologically resemble microglia, even though their origins are different [20, 32]. After injury, these cells participate in scavenging cellular debris *via* phagocytosis [20]. However, long term presence of macrophages can lead to chronic inflammation and leads to recruitment of new microglia and astrocytes. These cells are also known to form foreign body giant cells by fusing with each other and leading to cavitations near the injury [33]. Thus, similar to microglia, the excessive proliferation of macrophages must be managed and eventually down-regulated to allow microelectrode to interact with healthy neurons and ensure chronic recordings.

Finally, another important cell type that responds to brain injury is the astrocyte. Under normal conditions, astrocytes provide mechanical support and growth cues to neurons [34]. Astrocytes participate in multiple cell processes such as nutrient transport across the BBB, and regulation of chemicals required for neuronal function. Traditionally, activation of astrocytes take place one week after injury, followed by proliferation and migration to the injury site[35]. At this stage, the astrocytes become reactive and secrete nerve growth factor (NGF), which helps in repairing neural tissue [36]. The reactive astrocytes exhibit phenotypic changes characterized by hypertrophy and increase in expression of glial fibrillary acid protein (GFAP), which helps in cell repair [24]. However, these reactive astrocytes create a physical barrier between healthy tissue and the electrode, which interferes the ability microelectrodes to record from single neurons[37]. Thus, the accumulation of reactive astrocyte must be minimized in order restore tissue to its normal state following the insertion of the

microelectrode. As mentioned before, the exact timeline of cellular up-regulation following microelectrode insertion is not very well understood.

The overall goal of microelectrodes is to record single neurons. As reviewed in [38], in order to successfully record neurons, we must first understand how the density of neurons around the microelectrode changes over time. Secondly, we must also understand how does the increased glial cell production contributes to neuronal loss near the electrode. Tresco et al. suggest that microelectrodes lack the ability to obtain long-term *in vivo* recordings from neurons due to the death of neurons surroundings the electrode, and migration of neurons away from the microelectrode[8]. In another study, Biran et al. conclude that microglia activation leads to neuronal loss or vice versa [20]. They also suggest that neurons are displaced from the electrode site due to the recruitment of glial cells to the injury site [20]. The glial activation near the injury site lead to a "frustrated phagocytosis", a phenomenon where activated microglia continuously produce cytokines such as TNF α, IL-1β and prostaglandins, due to their inability to clear the insoluble microelectrode [20]. Other studies also report that mechanical damage occurs to the neurons as they are stretched, moved, pulled and torn between the migrating astrocytes [32].

The formation of the glial scar around the electrode has been studied extensively in number of studies. For example, Biran et al. observed the progression of glial scar following chronic microelectrode implantation compared to control animals which only received stab wound using the same type of device [20]. Using immunostaining techniques, they quantified the presence of macrophages, astrocytes, and neurons. After four weeks, the staining for neuronal nuclei (NeuN) showed ~40 % reduction in

number of neuronal bodies within 100 μm radius of the electrode. The primary reason for this reduction in neuronal density near the electrode is due to the presence of the glial scar, made up of astrocytes and glial cells. The authors also examined microglia/macrophage (ED1+), astrocyte (GFAP+) staining and found a higher amount of staining within 50μm radius of the device. The authors concluded that the astrocytes formed a sheath-like encapsulating layer surrounding the macrophage rich zone, with neurons being largely excluded from these zones.

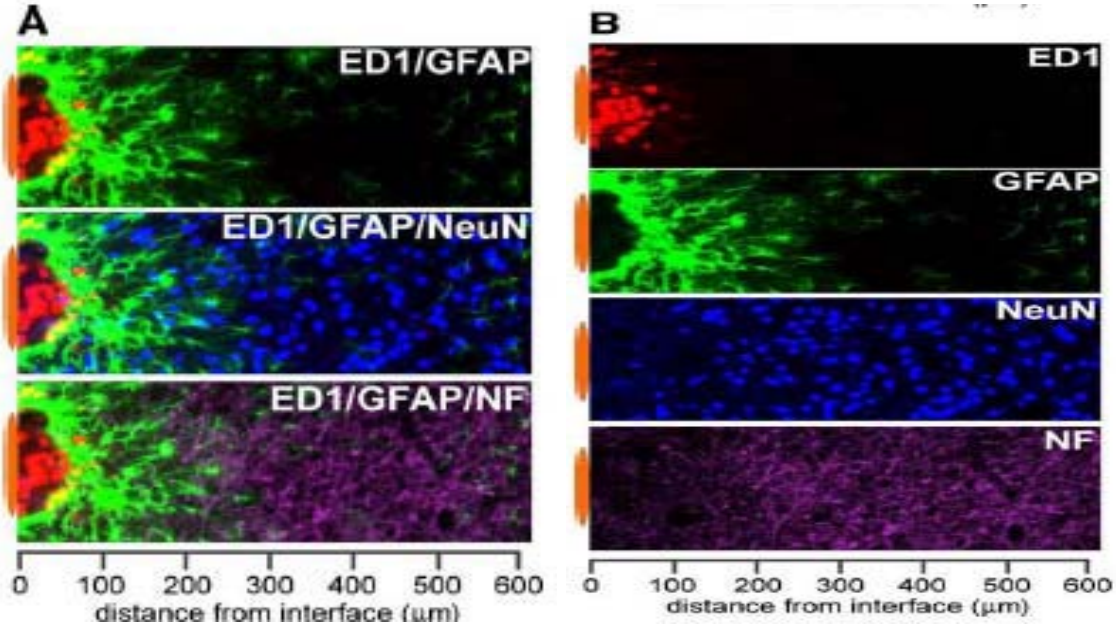

Figure 2.3: Immunostaining of macrophages, astrocytes and neurons after microelectrode insertion. (A) Overlapping images of inflammatory cells and Neurons after implantation for four weeks. (B) Individual images of each cell type after implantation (Reproduced from [20]) © Exp Neurol, vol. 195, pp. 115-26, Sep 2005.

2.2.4. Strategies to Minimize Host Reaction to Microelectrode Implantation

Several research groups are working on different strategies to minimize the tissue reaction to microelectrode implantation. As reviewed by Zhong and Bellamkonda, these approaches can be divided into two categories: materials science strategies and the bioactive molecule strategies[24]. The first strategy involves modifying the size, shape, and composition of the electrodes to minimize negative effects on the tissue from device insertion. Szarowski et al. studied both short term and long term effects of electrode shape, size, texture and tip geometry and their effects on the chronic tissue reaction to the microelectrodes [9]. They experimented with microelectrodes of 2500 μm^2, 10,000 μm^2, or 16,900 μm^2 cross sectional area and trapezoidal, square, or ellipsoidal cross sectional geometries. Furthermore, they also compared smooth surface textures, micrometer rough surface textures, blade or rounded tip geometries, and slow and fast insertion techniques [9]. Their results indicated that there is no difference in glial scar between any conditions after 6 and 12 weeks post-implant. Their results suggested that aspects other than mechanical factors must be examined to minimize tissue reaction. Additionally, the lack of quantitative measures makes it hard to fully explore their findings. Other material science approaches include using alternative materials for electrodes. Rousche et al. characterized polymer based multichannel intracortical devices and reported no changes in inflammatory response over long periods of time [39]. Other material based strategies include trying novel materials such as ceramics; however these showed no significant reduction of glial scar [40-41]. Recent studies have shown that modifying the surface of the microelectrodes to mimic

the extracellular matrix can enhance cell adhesion and facilitate charge transport between neurons and the recording sites of the electrode [17, 42]. This was shown in our previous work, nanostructured porous silicon microelectrodes decreased glial proliferation and increased neurite expression from PC12 cells *in vitro.* However, no improvement was seen in single neuron recordings or any significant reduction in the inflammatory tissue reaction *in vivo* [17, 43].

The bioactive molecule strategy involves minimizing tissue reaction *via* administration of anti-inflammatory agents by: direct injections using microchannels, systemic injections, or electrode coatings [24]. In a recent study, Retterer et al. have been able to incorporate microfluidic channels in order to deliver drugs to the insertion site, to help attenuate the host response to the injury [44]. Similarly, other studies utilized microfluidics to incorporate drug delivery channels into the microelectrode tips [45-46]. Multiple groups have been able to successfully implement microfluidic drug channels in to the microelectrodes and delivered labeled compounds into the tissue for short time periods [45-46]. However, these groups faced problems with fabrication as it was hard to incorporate these channels without increasing the size of the microelectrode tip. Also, no long term studies have been reported on the use of microfluidics to deliver drugs at the insertion site, making it hard to know if these channels can restore the normal cellular environment near the electrode.

A more basic approach reported in the literature is the use of biological compounds to modulate inflammation after injury. Using this approach, Koyoma et al. investigated the effects of BQ788, an endothelin ET_B receptor antagonist. Using this antagonist [47], Koyoma *et al.* were able to block the ET_B receptor expressed in reactive

astrocytes and microglia [47]. In injured rats, the induction of BQ788 showed a significant decrease in the GFAP staining as compared to control. However, the drawback to this study is that the authors only analyzed rats two weeks post injury. The effects of the antagonist must be observed for longer periods to show its potential in microelectrode application. Another anti-inflammatory compound that was investigated is the tumor necrosis factor-β1 (TNF-β1). TNF-β1, a strong inhibitor of astrocyte proliferation was administered to astrocytes *in vitro*[48]. The results showed a reduction of ~50 % in astrocytes when compared to control. Another biological compound, Protein S was shown to decrease the activity of astrocytes [49]. Plasma protein S added to glial cells after injury reduced the proliferation of reactive astrocytes by 50 % [49]. Induction of these different biological compounds show an inhibitory effect on astrocyte proliferation and further experiments need to be done *in vivo* to explore their potential.

Recently, many groups have reported that steroids have the potential to reduce inflammation after injury. Dexamethanose, a synthetic glucocorticoid has shown to have reduced astrocyte proliferation [12, 50]. In rats, a single dose of dexamethasone after implantation showed minimal amount of GFAP, CD11b and laminin staining after 6 weeks [50]. Similarly, when dexamethasone was injected on a weekly basis, comparable results were seen [50]. Shain et al. were also able to show reduced glial scarring after systemic doses of dexamethasone [51]. These results suggest that dexamethasone has the potential to regulate glial proliferation; however this comes with unwanted side effects. Kim and Martin suggest that dexamethasone along with other neurotrophic

factors can be used in drug delivering systems at the microelectrode implantation sites to address the problem of glial scar [52].

Finally another bioactive strategy that has been widely accepted to reduce inflammation near the injury site is by electrode coatings[24]. Bjornsson et al. conducted an *in vivo* study where poly (ethylene-co-vinyl) acetate (EVAc)-monocycline coated electrodes were examined [53]. Their results indicated that the coated devices elicited more severe response than uncoated devices. It was hard to conclude from their results what caused the failure of the coating. In another study, Wadhwa et al. coated the Michigan neural probes with polymer polypyrrole using dexamethasone phosphate as the negatively charged dopant [54]. Using electrical stimulation, the drug release was controlled over time. When these probes were tested *in vitro*, it was shown that the drug remained bioactive for long periods of time[54]. However, the efficacy of these coatings was not tested *in vivo*. Kim and martin reported a different coating strategy of DEX loaded nanoparticles embedded in alginate hydrogel as coating on the Michigan electrodes by dipping method [52]. *In vitro* studies using these coated devices have shown sustained drug release up to three weeks. And when implanted *in vivo*, the coating helped keep the impedance of the electrode relatively low [52] . In a different approach, He et al. tried to alleviate glial scar using laminin, a bioactive protein to alleviate glial scarring around the implant [13]. The authors created nano coatings of polyethyleneimine (PEI)-laminin and implanted into the cortex of the rats. Initially, there was no difference between LN-coated and uncoated probes. However after 4 weeks, the coated electrode had less glial activation showing that coating has reduced the accumulation of microglia and astrocytes. A different paper from the same group

reported an alternative strategy to reduce the glial scar [12]. Zhong et al. used dexamethasone coatings to attenuate inflammatory response and neuronal loss [12]. Their results indicate that initially dexamethasone shows reduced inflammation; however over time this difference between coated and uncoated electrodes was not significant. In conclusion, administration of anti-inflammatory compounds from microfluidic channels or electrode coatings has the potential to minimize the cellular and tissue response and therefore shows great promise to solve the problem of glial scarring of the chronically implanted microelectrodes. The research of this thesis will be focus on the bioactive coatings strategy using a neuroprotective agent, poloxamer- 188.

2.3. Poloxamer- 188 promotes cell repair

Neuroprotective agents are another type of bioactive approach to reducing the glial response to microelectrode insertion. After the initial insertion, the neurons suffer membrane damage that causes them to either die or recruit glial cells. Thus, a strategy was developed in order to help in recovery of damaged cell membrane after injury. In this thesis, we present poloxamer -188 (PLX) electrode coatings in order to promote neuronal survival. Poloxamer is a water soluble non-ionic surfactant with tri-block copolymer (MW 8,400) containing a central block (MW 1, 750) of polypropylene (29 PPO) moieties and two peripheral blocks (MW 3,500) of polyethylene (38 PEO) moieties each. This compound is not biodegradable and previously approved by Food and Drug Administration (FDA) as skin wound cleanser for use in human in 1978.

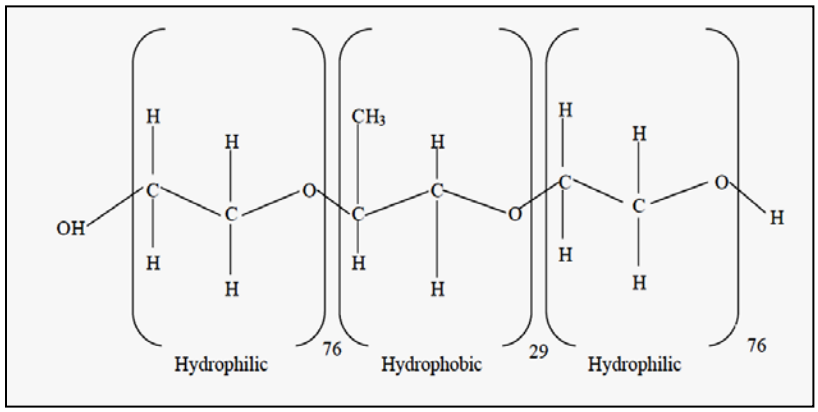

Figure 2. 4 : The chemical structure of poloxamer-188 (PLX)

Various studies have demonstrated that exposing damaged cells to this surfactant can effectively seal the damaged membranes of neuronal cells and other types of cells [55-56]. In 2001, Marks et al. showed that PLX is effective in repairing both non-neuronal and neuronal cell membranes after injury [55]. In their study, they reported that damaged hippocampal neurons were prevented from cell death when incubated in PLX. However, it was not clear whether PLX interacts only with the disrupted parts of the membrane to seal the membrane wounds or whether their integration and interaction with entire bilayer alters the membrane properties in a way to repair itself [57]. In order to understand this, Serbest et al. developed an *in vitro* model of traumatic brain injury to test the effects of PLX on damaged neuronal cells. They reported that when poloxamer was added to mechanically injured cells, it has been found to seal plasma membranes, promoting cell viability and subsequent recovery [11]. Results from the *in vitro* study showed that PLX promoted neuronal cell viability in a dose dependent manner[11]. Subsequently, a different study by the same group showed that treatment with PLX prevents post-injury axonal bead formation and enhances neuroprotection [57-58]. Since it was shown that PLX specifically targets

plasma membrane, it may help in healing of damaged neurons after electrode insertion. Therefore, we hypothesize that poloxamer could enhance neuron survival following electrode injury, aiding in the repair of neurons damaged during electrode insertion.

2.4. Measuring the immunological response

As outlined above, the insertion of a microelectrode leads to changes in cellular upregulation that causes the loss of recordings months after the implantation. It is important to have a standard approach to measure these changes in cellular level, which ultimately lead to the isolation of device from the healthy tissue. In order to find solutions that help reduce the cellular damage and ultimately obtain neuronal recordings, it is important to understand the brain's response to microelectrode at the cellular level. The development of various biomarkers allows for the possibility of assessing the changes at the cellular level. In their activated state, the cells involved in inflammation express certain proteins which can be labeled using immunohistochemistry. In order to assess the potential of our solution, immunohistochemistry can be used to evaluate the cellular response. In literature, proteins specific to microglia, macrophages, and astrocytes have been long identified [59]. In order to trace these proteins, a primary antibody that will bind to the protein will be used. Once the primary antibody has bound to the protein, a second antibody tagged with a detection agent is then added to bind to the primary antibody. This allows visualization under a microscope and further analysis [59]. Traditionally, the staining techniques were used to view one cell type at a given time on a tissue slice. However, recent advances have allowed viewing multiple cell types using antibodies that fluoresce under different wavelengths. For this study, primary antibodies were used to

stain for microglia, macrophages, astrocytes, and neurons as shown in table below. Using these stains, the difference in tissue response between coated electrodes and control ones can be useful to determine if the coatings have any effect and also in studying the effect on the proliferation of the immunological cells.

Table 1: Standard Primary Antibodies used to Identify Cells of Interest: (Microglia, Macrophages, Astrocytes and Neurons)

Cells of Interest	**Primary Antibody**
Microglia	ED1 (CD68)
Macrophages	ED1 (CD68)
Astrocytes	GFAP
Neuron Cell body	NeuN

3. Overview of Experimentation

In order to assess the effects of poloxamer coatings on tissue response after implantation, fifteen male, Long-Evans rats were anaesthetized and implanted with microelectrodes into the somatosensory cortex. The devices were implanted bilaterally into the two hemispheres of the rat's brain. One of the electrodes was coated by dipping with poloxamer and the control electrode was dipped into saline. After the implantation, the area was covered up with dental cement and the rat was allowed to recover. At 2, 4, and 6 weeks, five animals at each time point were sacrificed (Table 2).

The rats were euthanized at the respective sacrifice date and brains were extracted to prepare for perfusion. Rats were sacrificed with an overdose of euthasol and brains were perfused transcardially with phosphate buffered saline (PBS) followed by 4% paraformaldehyde. Perfused brains were cut into 20 μm using a cryostat and tissues were placed on slides. Tissue slides were treated with antibodies to stain for macrophages, neuron cell bodies, and astrocytes. Once the tissue samples were treated with staining antibodies, two quantification methods were applied (see methods section). Macrophages, microglia, astrocytes, and neurons were analysed in each animal by counting cells in 4 -5 slides using the steroinvestigator software. In astrocytes, the hypertrophy was characterized by intensity analysis developed using MATLAB software. A three way ANOVA model was then used to analyze the differences between PLX coated and uncoated electrodes in terms of inflammatory cellular response and neuronal presence.

Table 2 : Summary of Experimental conditions - experimental setup of microelectrode implantation at two, four and six weeks.

					Implant Side
Rat Number	Time points	Electrode Type	Surgery Date	Perfusion Date	(PLX, Control)
PLX3	4 weeks	PS-19	8/25/2008	9/23/2008	Left, Right
PLX4	2 weeks	PS-19	9/9/2008	9/23/2008	Left, Right
PLX6	2 weeks	PS-19	9/11/2008	9/24/2008	Left, Right
PLX7	6 weeks	PS-19	9/14/2008	10/28/2008	Left, Right
PLX8	6 weeks	PS-19	9/18/2008	10/28/2008	Right, Left
PLX10	6 weeks	PS-19	4/5/2009	5/17/2009	Left, Right
PLX13	4 weeks	PS-19	4/26/2009	5/31/2009	Left, Right
PLX14	4 weeks	PS-19	5/7/2009	6/7/2009	Left, Right
PLX15	4 weeks	PS-19	5/10/2009	6/7/2009	Right, Left
PLX18	2 weeks	PS-19	5/21/2009	6/7/2009	Left, Right
PLX19	2 weeks	PS-19	5/27/2009	6/14/2009	Right, Left
PLX20	2 weeks	PS-19	5/24/2009	6/14/2009	Right, Left
PLX21	6 weeks	PS-19	7/16/2009	8/27/2009	Right, Left
PLX22	6 weeks	PS-19	8/6/2009	9/17/2009	Right, Left
PLX23	4 weeks	PS-19	8/13/2009	9/10/2009	Right, Left

4. MATERIALS AND METHODS

4.1. Microelectrodes

Porous structure ceramic-based, multisite electrode (CBMSE) arrays were fabricated according to methods previously described by Moxon et al. [5]. The porous silicon surface is fabricated *via* stain etching. Silicon wafers, n-doped, single side polished, 0.1-10 ohm-cm resistivity, and 200 micron thick were used to create nanostructured porous structured electrodes. Thin film photolithography was used to pattern the microelectrodes (4 recording sites) and ion-beam assisted deposition of alumina was used to insulate the individual electrodes. Microelectrodes were diced according to methods in our previous study [17]. Each electrode had four recording sites spaced 0.2 mm apart at the tip of the electrode. Each recording site was 22 μm x 80 μm. The width of the electrode at the tip was 66.4 μm and width of the array at the opposite end near the final recording site was 113 μm. The electrodes were 7 mm in total length and 200 μm wide at the base. All electrodes were sterilized prior to implantation by exposure to isopropyl alcohol and sonication for 5 minutes first in DI water and then isopropyl alcohol.

4.2. Implantation of Microelectrodes

All animal procedures were performed utilizing sterile techniques approved by Drexel University Institutional Animal Care and Use Committee (IACUC) and adhered to National Institute of Health (NIH) guidelines. Adult male Long-Evans rats between 275-299g were used in this study. Prior to surgery, animals were anesthetized using 4.5 %

isoflourane in oxygen at 1 L / min. The rat's head was shaven and the area of interest was disinfected with an isopropyl alcohol followed by a butadiene swab. Ophthalmic ointment was applied to animal's eyes to prevent drying. Each animal was placed on a stereotactic frame and anesthesia was maintained in oxygen in 0.2 L/min for the duration of the surgery. A midline incision was made in the skin and the skull was centered to bregma on the stereotax. The coordinates were zeroed to bregma and a 3mm craniotomy was drilled for each of two electrodes at +1 mm bilaterally, + 2.5 and -2.5 mm anterior to bregma. In order to support the electrode cap, a series of smaller anchoring points were drilled in skull for placement of four metal screws. The bone plug of the craniotomy was carefully removed and the dura was gently pierced with fine microforceps. Immediately prior to insertion, one of the electrodes was coated with poloxamer by dipping it twice for 5 min in a 100 μM Poloxamer 188 solution (Sigma) dissolved in DI water and the control electrode was dipped in saline. The microelectrodes were then air dried for 10 minutes between coatings and inserted through the pia layer at a rate of 5μm/min into the cortex at a depth of 2mm. Throughout the surgery, saline was applied to restrict exposure of brain while electrode insertion and to minimize iatrogenic damage. After insertion, the craniotomy was covered with dental acrylic. The skin incision was then closed with surgical staples and the animal was allowed to recover from anesthesia on a heat pad at 20° C. Animals were monitored every 2 hours until they fully recovered from anesthesia, and then once per day for the remainder of the study.

4.3. Tissue processing for immunohistochemistry

To measure the effects of surface coating, animals were euthanized at, two weeks, four weeks, and six weeks post implantation. The rats were sacrificed with an overdose of Euthasol and then perfused transcardially with 0.5 L of ice cold PBS followed by 0.5 L of ice cold 4% paraformadelhyde. The brains were removed such that the implanted neural probes remained intact. After post-fixation of the brain in paraformaldehyde for 48 hours, the brains were dissected and the electrodes were carefully retrieved from the tissue. The brains were placed into 30% sucrose in PBS solution (4° C) to equilibrate for three to five days. After the equilibration period, the tissue was frozen and cryostat sections of 20 μm thick were cut in using Leica CM3500 cryostat the in the horizontal plane. The sections were collected using low-distortion tape system serially and sorted into three sets and mounted onto slides, while maintaining dorsal to ventral order[60].

4.4. Immunohistochemistry

Sections from cortex were stained simultaneously to observe brain tissue response. After cortical sections were mounted onto the slides, the slides were ringed with rubber cement to create wells and treated with antibodies to stain for cells of interest. Sections were washed in PBS and blocked in goat serum for an hour at room temperature. Sections were then incubated overnight with primary antibody applied at a 1:1000 dilution. Group one received mouse monoclonal ED1 (Serotek, 1:1000) to stain for reactive macrophages and microglia. The second group received mouse monoclonal anti-NeuN (Chemicon, 1:1000) to stain for neuron cell nuclei, and group three received

rabbit polyclonal anti-glial fibrillary acidic protein (GFAP, Sigma, 1:1000) to identify astrocytes. After the incubation, sections were washed in PBS and incubated in secondary antibodies coupled to FITC or TRITC (Jackson Immuno Research) for two hours at a 1:100 dilution. All of the sections received a nissl counter stain. The tissue sections were then washed again and coversliped with Vectashield to help preserve the tissue and prevent fluorescence degradation.

4.5. Qualitative Analysis

4.5.1. Stereological techniques

Design-based stereology was used to characterize the cellular presence in the histological sections. It is a method in which a three-dimensional interpretation of structures can derived from observations made in two-dimensional sections[61]. Unlike traditional methods, stereology does not rely on the information about the size, geometry, and orientation of interested cells types therefore resulting in a more accurate cell count[61]. In contrast to the commonly used geometry models, design based stereology is an assumption free method and can be used to study objects of different shapes. In this study, cell counts were performed using Nikon microscope attached to a Zeiss Axioplan, which was connected to a Dell workstation using Steroinvestigator Software (Microbrightfield, Inc, Williston, VT). A motorized stage was controlled by the software suite to allow for precise tracking along the x and y and z axes. Sectioned tissue samples were observed at a magnification of 2.5X. The center of each electrode hole was located and the coordinates of this point were marked as a reference. Using a contour tool a circle of 500 μm radius was traced around the

electrode hole. An optical fractionator probe was then assigned to each fluorescent antibody of astrocytes (GFAP), neurons (NeuN), and microglia (ED1) at high magnification of 100X (1.30 NA) oil objective. This probe denotes cells observed by using optical dissector and combing it with a fractionator sampling for the estimation of population size. A sampling grid was generated within the traced contour and an unbiased counting frame was determined within each sampling domain such that acceptance and rejection criteria guaranteed that cells would only be counted once. The sampling grid and counting frame dimension were chosen to create a 17.3% sampling percentage within the selected contour. At each sampling site, the tissue was scanned in the Z axes, and cell presence was acknowledged when the nucleus came into focus. The counting frame area was selected to be 2500 μm^2 (in X, 50 μm; in Y, 50 μm) and the grid size of 0.0144 mm^2 (in X, 120 μm; in Y, 120 μm). The optical disector height (thickness) was set at 12 μm with a 4 μm top and bottom guard zone. To avoid estimation errors, cells are not counted within the guard zone area located at the top and bottom sides of the counting frame. An advantage of this method is that it estimates the total number of objects in any three dimensional volume regardless of that volume's shape and therefore is unaffected by tissue shrinkage that tends to occur during tissue preparation. All of desired cell types (astrocytes, microglia, and neurons) were counted around the treated electrode hole and the control hole for animals at 2, 4 and 6 weeks.

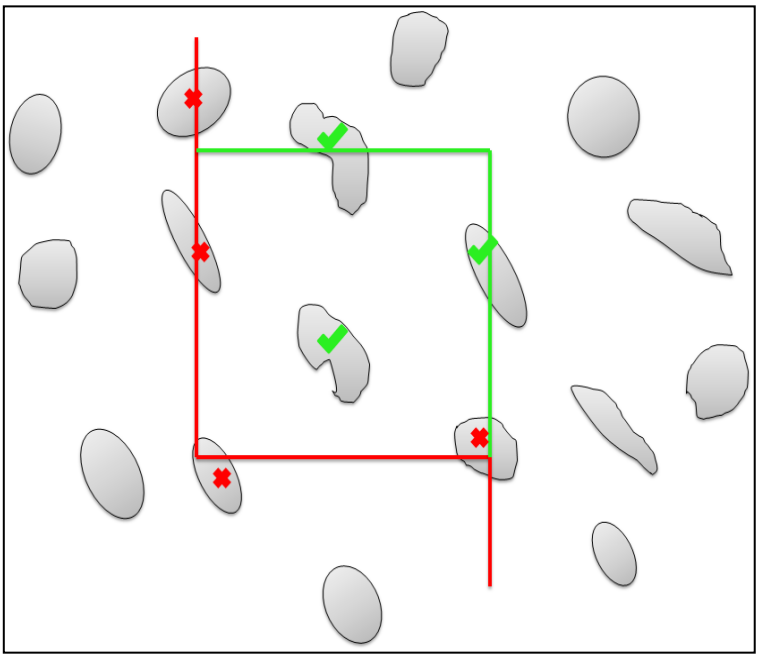

Figure 4. 1: An illustration of a counting frame and a number of differently shaped cells. The check marks in green show the particles that are counted and the check marks in red show why some of the cells are not counted.

4.5.1.1. Cell Density Profile Across Distance

During cell counting, the coordinates of each cell were recorded with respect to the center of the electrode and the radial distance was determined in μm. The cells were binned in 5 annular domains based on distance from the center of the electrode hole: 0-100 μm, 100-200 μm, 200-300 μm, 300-400 μm, and 400-500 μm. The total number of cells in each annular domain was normalized by dividing by the number of counting frames within each annular domain. The number of counting frames within each domain was determined geometrically, using a trapezoidal approximation for counting fames spanning more than 1 domain by developing a custom program in Matlab. In order to account for tissue loss during explanation, the counting frames were not

included in the analysis if there was no tissue present in any part of the bin. Using the normalized cell count, the cell density at each bin was determined by dividing by the volume of each counting frame (Figure 4.2). Additionally, the overall cell density around the 500 µm region of the implant side was calculated. The overall cell density and density at each bin was analyzed for ED1, GFAP and NeuN stains and compared between coated and non coated electrodes using a univariate ANOVA model.

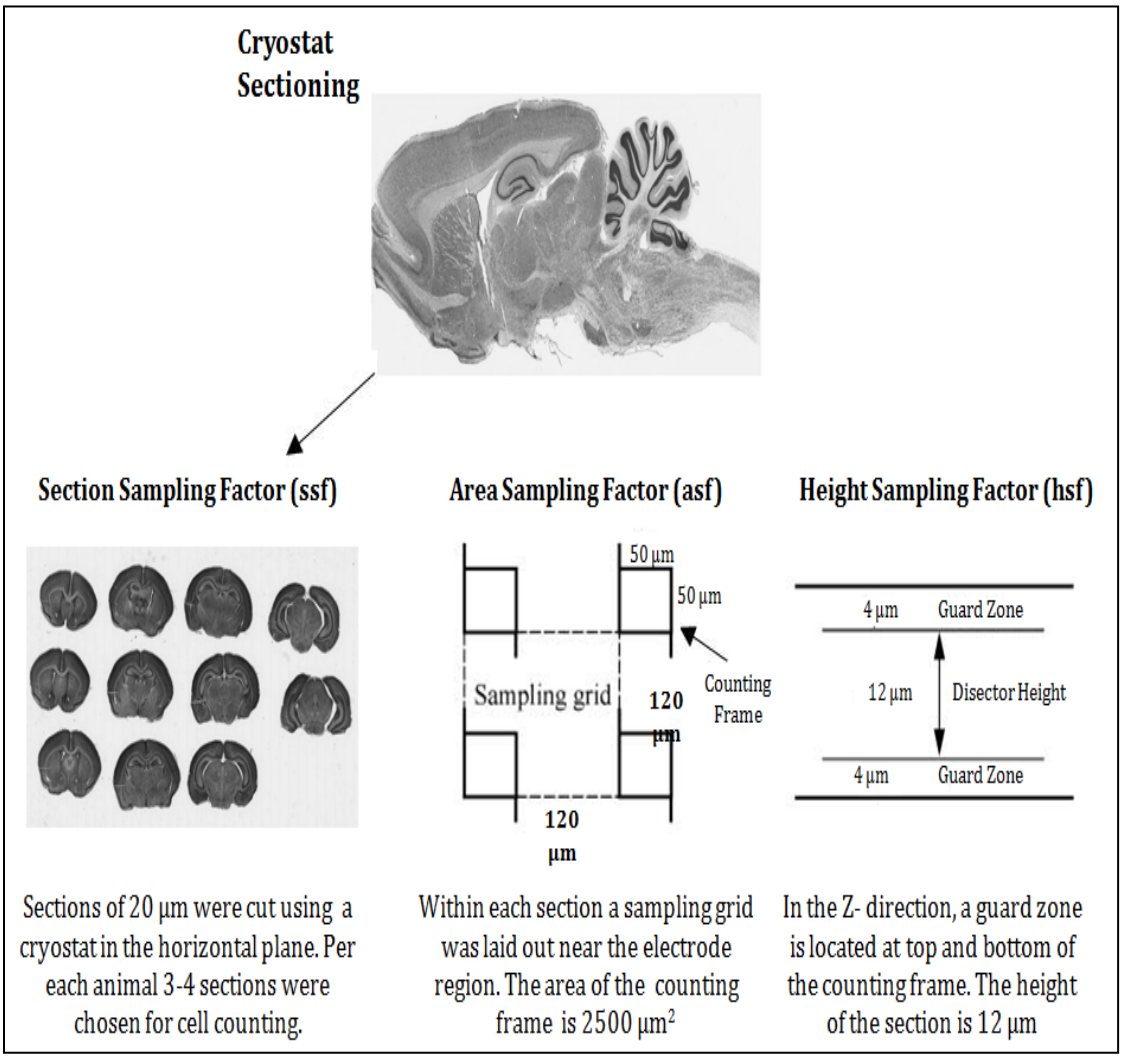

Figure 4.2 : Random systematic sampling is applied to estimate the total number of cells (N) near the electrode. Images courtesy of Dr. Nissanov, Drexel College of Medicine

4.5.2. Intensity analysis

When astrocytes are upregulated they not only increase in number, but also increase in size. Using cell count based methods would not provide information regarding the hypertrophied nature of these reactive astrocytes. Therefore, an intensity based method was developed to assess the hypertrophied character of GFAP expressing cells. Using the microscope setup described above, the fluorescent images were acquired for GFAP marker at 10X magnification around the electrode. Image analysis was then performed using a custom program developed in MATLAB to assess images of the tissue surrounding the implant. In this program, a grid of ten equidistant lines was superimposed on the image and the position and orientation with respect to the hole was random. Using a consistent intensity scale, the intensity of staining was quantified across the ten lines to determine the intensity profile across the distance. For all of the images, the edge of the hole was estimated using a graphical representation of the intensity. From this edge, average fluorescent intensity across a distance of 200 μm was calculated with four intervals at 50 μm, 100 μm, 150 μm and 200 μm. To account for variations in staining intensity between subjects, the background staining was removed by calculating the intensity of staining in tissue away from injury and subtracting this level of intensity.

4.5.3. Hole Size Analysis

Since some tissue was lost during electrode extraction, the tissue loss was calculated in both coated and uncoated conditions. Fluorescent images were taken at

2.5x magnification around the implant site and then converted into grayscale. ImageJ software (National Institutes of Health) was used to analyze the relative hole sizes on the images and a student's t-test was used to compare the differences between coated and uncoated electrode holes.

4.5.4. Statistical Analysis

Data are represented as the average value ± the standard error of the mean (S.E.M). A three way ANOVA model was used to compare the mean values of different conditions using $p < 0.05$ for significance. The first factor was condition with two levels: PLX coated or non coated. The second factor was time post-implant with 3 levels: 2, 4 or 6 weeks. The third factor was distance from the microelectrode with 5 levels: 0-100 µm, 100-200 µm, 200-300 µm, 300-400 µm, 400-500 µm. Post-hoc, pair wise comparisons were conducted using Students t-test analysis (2-tailed). A Bonferroni correction method was to used to assess multiple comparisons, up to 5 as described in the results, and the p-value was reduced to $p< 0.01$ (0.05/ n, where n = number of comparisons) was used to indicate statistical significance.

5. DESIGN COMPONENT

5.1. Problem Statement

Most of the earlier studies that examined the up-regulation of inflammatory cells around the microelectrode were primarily qualitative. However, in order to understand tissue response after microelectrode insertion, quantifying the astroglial upregulation is crucial. Although cell counting and intensity based methodologies have been utilized in the past, very few studies have incorporated both. It is important to utilize both as upregulated cells not only increase in number but also exhibit hypertrophy. Recent studies in literature have solely used intensity methods to quantify the glial scarring around the implant. The problem however is that the intensity methods misrepresent cell counts due to variations in cell size, shape and volume. Thus, there is a need to apply a true stereology approach and design a new method to assess glial scarring. Additionally there still needs be a combination method to quantify astrocytic cell response. The counting of astrocytes cells is difficult because the GFAP stain labels the processes of the astrocyte as well as the cell body, making it hard to discriminate one cell from another. Therefore, a method is required which incorporates quantification of cell count as well as their hypertrophied nature.

5.2. Design Criteria

- The aim of the design method is to quantify the cellular response around (500 μm) the implant hole. Thus, the method must be able to quantify microglia / macrophages, astrocytes, and neurons around the implant site.
- The design method must be able to quantify cellular response in terms of both cell proliferation (number of stained cell) and cell hypertrophy (intensity of the staining).
- The design method must account for tissue loss during tissue processing and avoid any artifacts due to tissue shrinkage over time.
- The design must be able to quantify inflammatory response and neuronal presence near the electrode (0 – 100 μm) and also far from electrode (400 – 500 μm).
- Reproducibility of the quantification protocol will be important and variability must be at a minimum, if any.

5.3. Proposed Solution

5.3.1. Design based Stereology protocol

Design-based stereology is a method of interpreting three-dimensional structures based on observations made in two-dimensional sections [14]. Unlike traditional methods, design based methods eliminate the need for information about the geometry of interested cells types therefore resulting in a more accurate cell count [14]. A protocol was developed using design based stereology, where cell counting is

unbiased and random resulting in more robust data. Once the 20 μm brain tissues are sectioned using a cryostat, they are put on a cover slide and observed under a fluorescence microscope. The center of the electrode hole was located and the coordinates of this point were set as zero. Using a contour tool, a circle (500 μm radius) was traced around the electrode hole. The objective was to count the number cells in the traced region of interest. Using Stereoinvestigator 7 software, an optical fractionators probe was designed to quantify cell types. This probe estimates the total number of objects in any three dimensional volume regardless of that volume's shape. The program allows us to select a series of randomly sampled sections and then sampling each section in X, Y, Z axis. The counting frame in each site is defined with acceptance and rejection regions to guarantee that each cell is only counted once (Figure 5.2). A pilot study was performed to determine the optimal grid size, counting frame, and a guard zone of the dissector. The counting frame area was selected to be 2500 μm2 (in X, 50 μm; in Y, 50 μm) and the grid size of 0.0144 mm2 (in X, 120 μm; in Y, 120 μm) giving a 17.3 sampling percentage. The optical dissector height (thickness) was 12 μm with a 4 μm top and bottom guard zone

In each sampling site, once a cell is observed the coordinates of the cell are marked, and using Pythagorean Theorem the distance of each cell from the center point will be calculated. The distances from the center of the hole were then binned into 5 domains: 1-100 μm, 100 - 200μm, 200 – 300 μm, 300-400μm, and 400- 500μm. Next, using Microsoft excel the total number of cells in each bin were then calculated. One of the problems using this approach is that the data needs to be normalized. This is due to the placement of sampling grid, as there are more sampling boxes far away from the

center. Thus, we decided to normalize the counts in each bin by dividing with number of sampling boxes in order to give us an average cell count per sampling box. In order to do this, we needed to exactly figure out how many sampling boxes were in domain. To determine this, we used a custom build program in Matlab. On the stereoinvestigator software, the coordinates of each square sampling box were marked and recorded. These coordinates were then used to build a Matlab program, in which the total number of counting boxes in each domain was determined geometrically, using a trapezoidal approximation for counting fames spanning more than 1 domain. The program was able to calculate the exact number of bins in each domain (Table 2). Once the normalized cell count in each bin is calculated, the cell density is determined by dividing it by the volume of the counting frame (50 μm * 50 μm * 12 μm).

An advantage of using the stereology method is that we can quantify the total density within the 500 μm region of interest. Generally, quantifying the number of cells within a region is complicated, as it usually not possible to isolate cells. Thus, it is necessary to cut the tissue into section, to find the number of cells within that section and estimate based on that. Design based stereology allows us do this via the optical fractionator method. The estimate of the total cell density in the region was obtained by dividing the total number of cells counted in the region by (total counting frames * volume of the counting frame). The volume of the counting frame is defined by the volume of rectangular solid (50μm (height) * 50 μm (width) * 12 μm (depth)). In order to account for tissue loss during immunostaining, the counting frame was not included in the analysis, if tissue was not present in the frame. Once the tissue slides for poloxamer coated electrodes and control electrodes are analyzed, a t-test and

multivariate ANOVA was performed to observe any significant difference between the two.

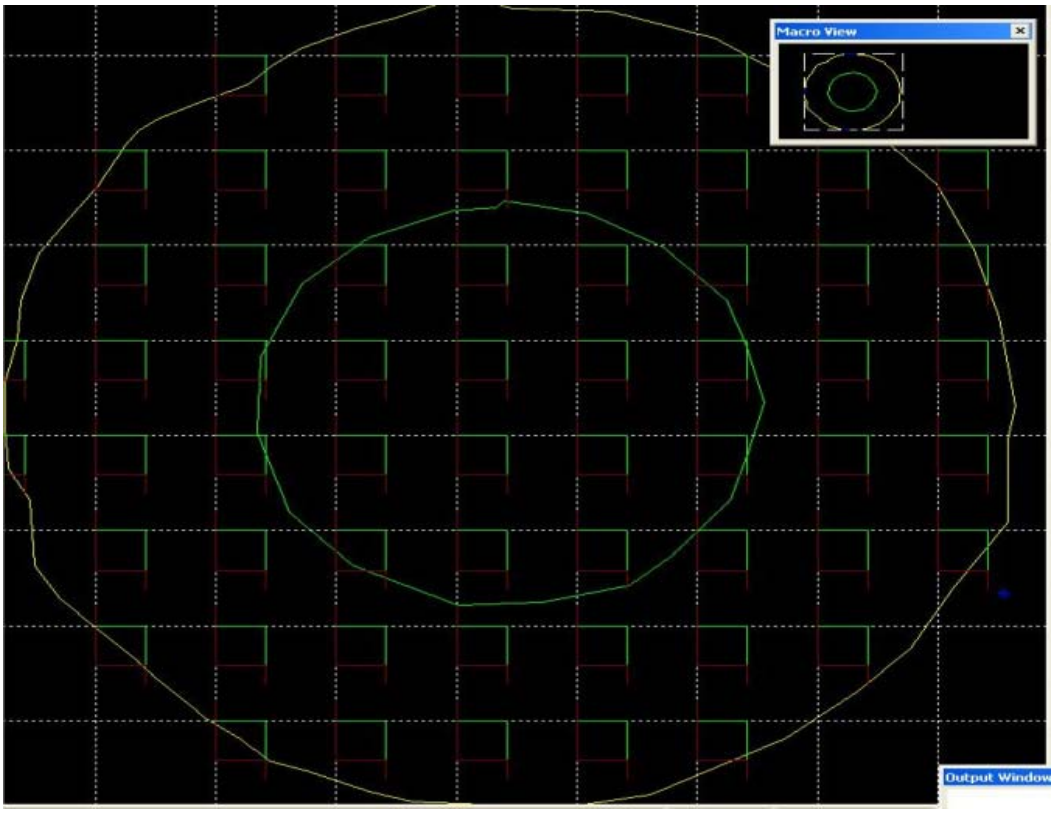

Figure 5. 1 : An illustration of a sampling grid placed around the electrode hole .Each gird contains a series of sampling domains with a counting frame. Within the counting frame, sampling was enabled in X, Y, Z axis. Each counting frame had an acceptance region (green) and a rejection region (red).

Table 3: The number of counting frames was determined in each domain using a custom build Matlab program

Domain	Number of counting frames
0 – 100 µm	1.5305
100 – 200 µm	7.178
200 – 300 µm	11.7292
300 – 400 µm	15.3939
400 – 500 µm	18.6331

5.3.2. Intensity Analysis Protocol

Our method for quantifying astrocyte hypertrophy was primarily based on work done by Biran et al. and other studies reported in literature [12-13, 20]. Using a horizontal line intensity analysis, the image of the tissue surrounding the implant was quantified. The reason for applying an intensity based analysis is due to fact that GFAP staining in astrocytes is proportional to the level of hypertrophy. Cell counting can also be utilized to quantify these cells; however it is difficult in identifying $GFAP^{+}$ cells leading to miscounts. Thus, we chose to have both cell counts and line intensity spectrum of magnitude of staining along a horizontal line across the image. The intensity from these lines can be average and statistically analyzed to determine the differences between coated and uncoated electrodes

In order to quantify the intensity, images of GFAP stained tissue at 10X magnification were taken to the right and left of the electrode hole. The program was developed in a way that the user must specify whether the image was to the right or left side of the tissue. Once this image is specified, ten random lines are placed across the image and the intensity of the staining is calculated based on an intensity scale predefined by user (Figure 5.2). This intensity is calculated for each pixel and an intensity profile is generated across the image. Using the graphical representation of the intensity, the user will determine the edge of the hole and zero the data at this edge. Establishing a zero point is important because it allows for calculating intensity at a given distances from the edge of the microelectrodes. Additionally zeroing all of the data at this point negates the lack of intensity in the hole, as there is no tissue. An advantage of calculating intensity from the edge of hole eliminates intensity artifacts or loose tissue in the space of the hole. Once the intensity profile is obtained and zeroed, the data from these ten lines is averaged and statistically analyzed to determine the effects of the PLX coatings. A three-way ANOVA model was used to assess the effect of poloxamer coatings as a function of distance from the hole. At two, four and six weeks post implantation, the difference between coated and uncoated electrodes was assessed using a paired t-test because each animal had both types of electrodes.

5.4. Design Constraints

- Since the design was based on fluorescent staining, there could be variations of intensity between different days of staining and image capture. Therefore, with different background intensity on different days, cross comparison of the different groups of images may be hindered.
- The cell counting protocol was used to quantify cell around the hole, however the size and geometry of the electrode hole is different. Even though this was accounted by not including counting frames where there was no tissue, there could be some missing data.
- The sampling grid used in the cell counting method is not uniform as there are more sampling sites far away than near the electrode. This is due to the circular geometry of the region of interest.
- The use of horizontal lines in the intensity analysis program do not yield the true radial distance as the electrode tracks are roughly circular. A better way to approach this would be to implement the use of radial lines in an automated fashion. This radial line method was not feasible for this work due to lack of appropriate software.

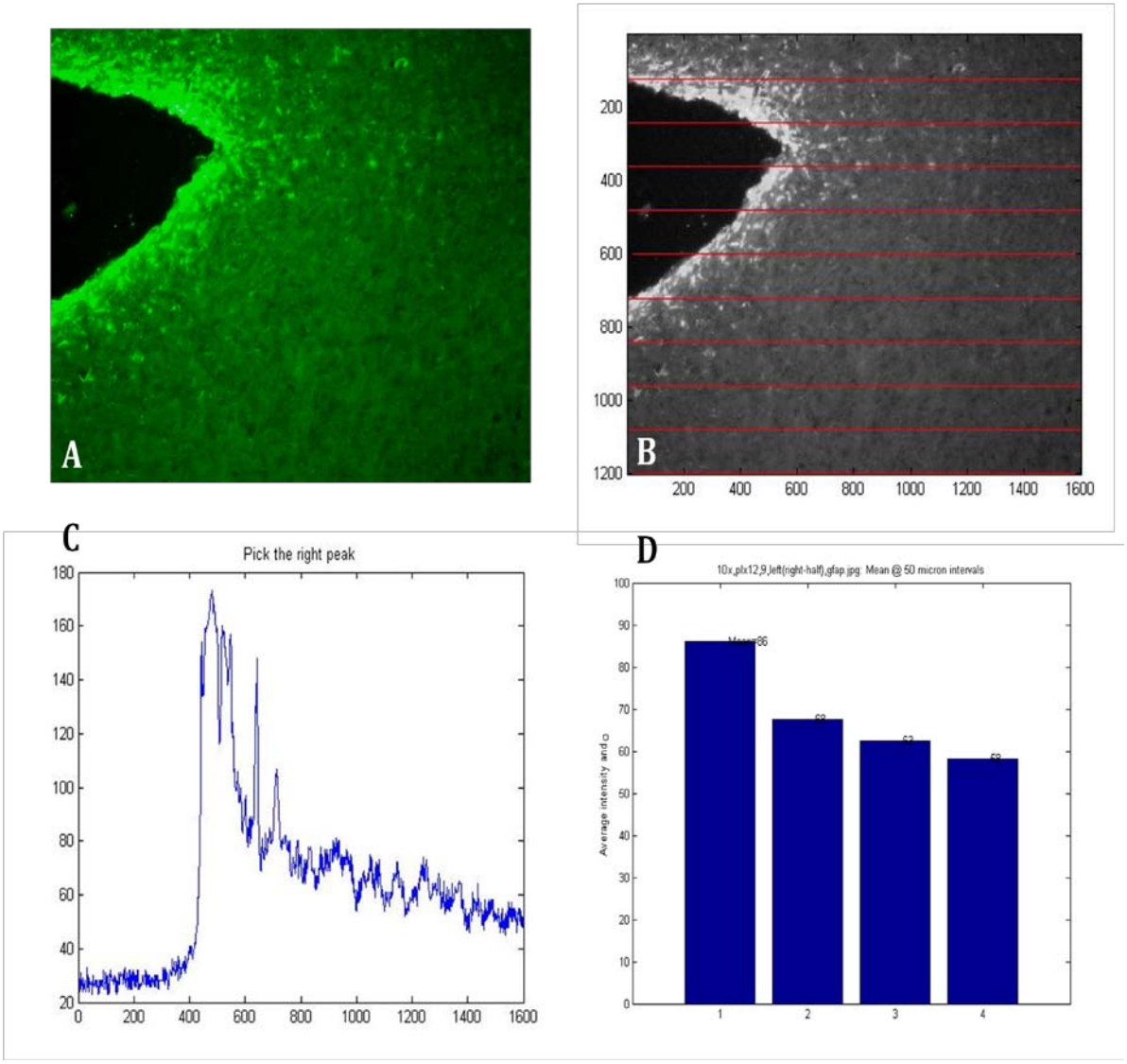

Figure 5.2 : A schematic of the intensity based analysis of GFAP staining using MATLAB: (A) Images of tissue around microelectrode are taken on the microscope at 10X magnification. (B)The image is converted to grayscale and the program randomly places ten lines (shown in red) on the image. (C) Across each pixel, the intensity profile across the horizontal lines is displayed as a graphical representation. In order to account for tissue loss during histology, the user must pick the edge of the hole, which is characterized by a very low intensity followed by large peak. (D) The intensity is then averaged and plotted onto a bar graph.

6. RESULTS

6.1. Characterization of tissue loss

Since we were analyzing the inflammatory response around a defined area near the electrode, the tissue loss was examined around the electrodes. The fluorescent images were analyzed using ImageJ software and area of the tissue loss was measured. The percentage of tissue loss as compared to control was measured in all of the brain sections (Figure 1). At two weeks, the tissue loss was slightly higher in coated electrodes. In contrast, the four week electrodes showed higher amount of tissue loss in the control devices. Finally six weeks post implantation, there was no difference in tissue loss between the coated the uncoated electrodes. Statistical analysis showed no difference in tissue loss between the two conditions ($p < 0.05$) at any time point, suggesting that coating has no influence on tissue loss.

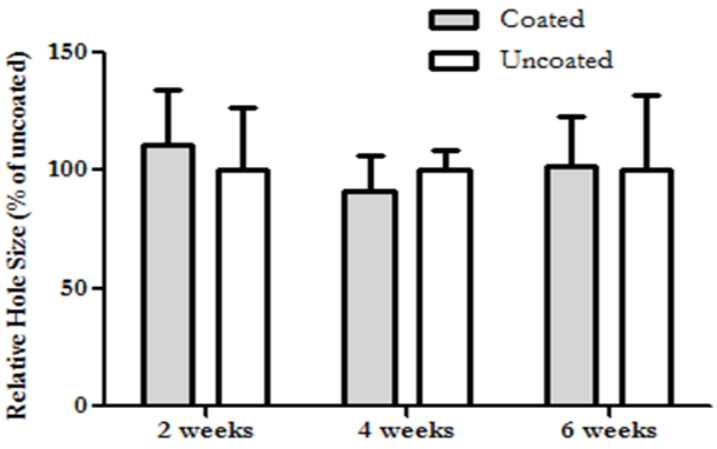

Figure 6. 1 : The percentage of tissue loss of coated compared to uncoated was plotted. No significant difference was observed between conditions at the 2 week, 4 week, and 6 week time points.

6.2. ED1 immunoreactivity

Activated microglia and macrophages were quantified around the electrode using ED1 staining. The amount of ED1 staining adjacent to poloxamer coated surface was significantly greater than the staining around the uncoated surface ($p < 0.001$, $F = 42.435$, $N= 490$). The ANOVA shows that as the distance away from electrode increased, there was a significant difference in the cell density ($p < 0.001$, $F = 65.681$ $N= 490$), suggesting cell accumulation near the electrode. Also, the analysis of variance demonstrated that as the distance from electrode increased, macrophage response was different in the PLX coated, when compared to uncoated electrodes ($p < 0.001$, $F = 9.901$, $N= 490$). That is to say that as the distance increased, coated sample elicited less response than the uncoated one. Finally, a significant interaction was found between duration of implant and type of electrode (coated vs. uncoated) ($p< .001$, $F = 6.757$, $N= 490$), suggesting that microglia response varied near the electrode as duration of the implant progressed *in vivo*.

Two weeks after implantation, the area around the coated electrode was characterized by faint diffuse staining with few ED-1 positive cells (Figure 6.2). In contrast, the staining around the uncoated electrode showed a significant increase in the number of ED-1 positive cells. Using Stereoinvestigator software, overall density of the tissue around electrode was quantified. After two weeks of implantation, the total density of ED-1 cells around the uncoated electrode was significantly higher ($p < 0.01$) than the poloxamer coated device (Figure 6.2-C). In order to further assess the cell response, the microglial cell density ($ED1^+$) was binned in 5 annular domains, 0 - 500

μm in 100 μm increments, based on distance from the center of electrode hole. Normalized ED1 cell density was significantly higher near the uncoated electrodes from 0- 400 μm, as compared to coated electrodes ($p< 0.01$) (Figure 6.2-D). Additionally, the difference in ED1 response within 0-100 μm between the two conditions was much higher than in the other bins. For both coated and uncoated devices, the cell counts peaked at 0-100 μm and rapidly decreased thereafter. This result is similar to other studies that reported an increase in glial activation near the microelectrode.

Four weeks post-implantation, the responses between coated and uncoated were similar to that of two week period. The majority of the $ED1^+$ cells were still located near the electrode and had the appearance of large, round blood borne macrophages (Figure 6.3). At this time, significantly higher numbers of $ED1^+$ cells were present around the control electrode in all of the bins except 100 – 200 μm (Figure 6.3-D). Likewise, the difference in overall cell density between the uncoated electrodes and PLX coated electrodes was statistically significant ($p<0.01$) (Figure 6.3-C). Overall, at four weeks, the same trend of relative difference between coated and uncoated response persisted as seen earlier. However, at this time point the microglial inflammation around the PLX coated device increased, when compared to earlier time point.

At six weeks post-implantation, the difference in cell density between the uncoated and PLX coated devices was no longer statistically significant (Figure 6.4). After six weeks, microglial cell density reduced near the electrode when compared to 2 weeks for both poloxamer and control conditions. Immunostaining of ED-1 shows more compact cells at this time, as opposed to amoeboid microglia/macrophage shaped cells seen at 2 and 4 weeks, implying macrophage senescence and stabilization. The cell

density distribution profile across the distance continued to be more uniform than earlier time points, but the overall cell density near the coated electrode rose to be even with the control. This suggests that effect of poloxamer diminished over time and is not sufficient to alter the *in vivo* up-regulation of glial cells after 6 weeks.

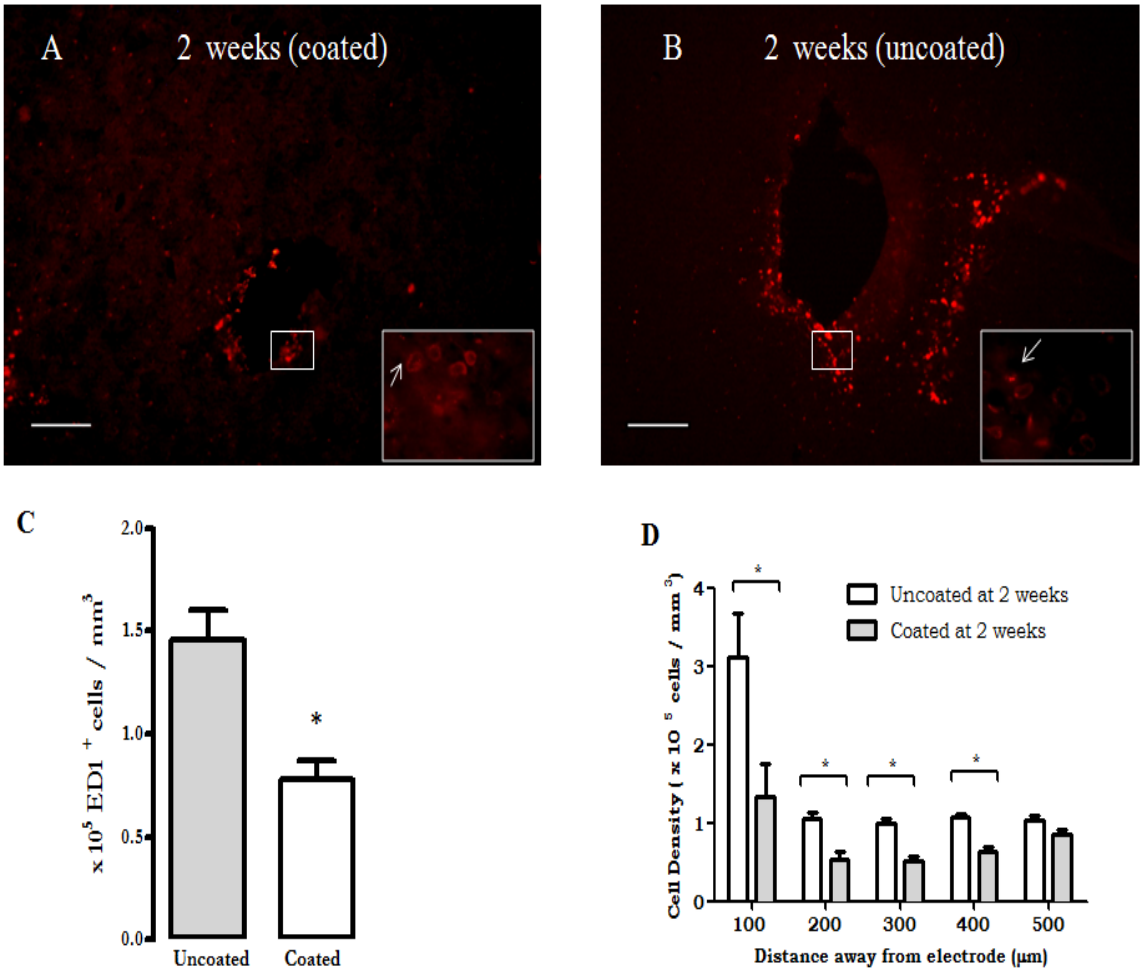

Figure 6. 2 : Quantitative cell density analysis of ED1 staining. (A) – (B) Representative images of ED1 staining for reactive microglia/ macrophages in the brain section 2 weeks post implantation for both coated and uncoated microelectrodes. Scale bar = 100 µm. (C) Estimation of overall ED1 cell density at 2 weeks post implantation(D) $ED1^+$ cell density profile as a function of distance at 2 weeks post implantation. Statistical differences between uncoated and coated probes at the same time point are indicated by * ($p < 0.01$ comparing uncoated to the coated electrode)

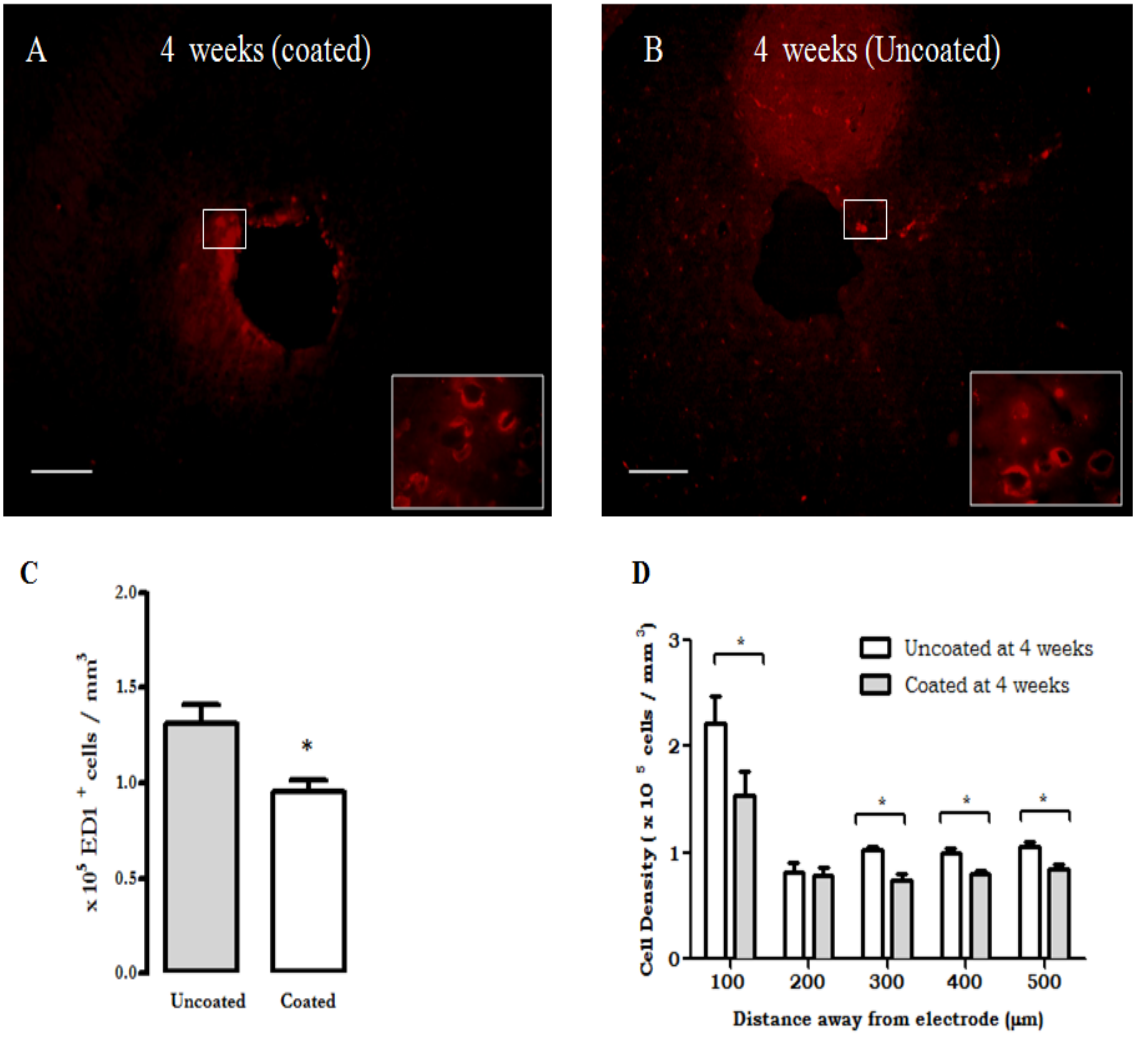

Figure 6. 3 : Quantitative cell density analysis of ED1 staining. (A) – (B) Representative images of ED1 staining for reactive microglia/ macrophages in the brain section 4 weeks post implantation for both coated and uncoated microelectrodes. Scale bar = 100 µm. (C) Estimation of overall ED1 cell density at 4 weeks post implantation. (D) $ED1^+$ cell density profile as a function of distance at 4 weeks post implantation. Statistical differences between uncoated and coated probes at the same time point are indicated by * ($p < 0.01$ comparing uncoated to the coated electrode)

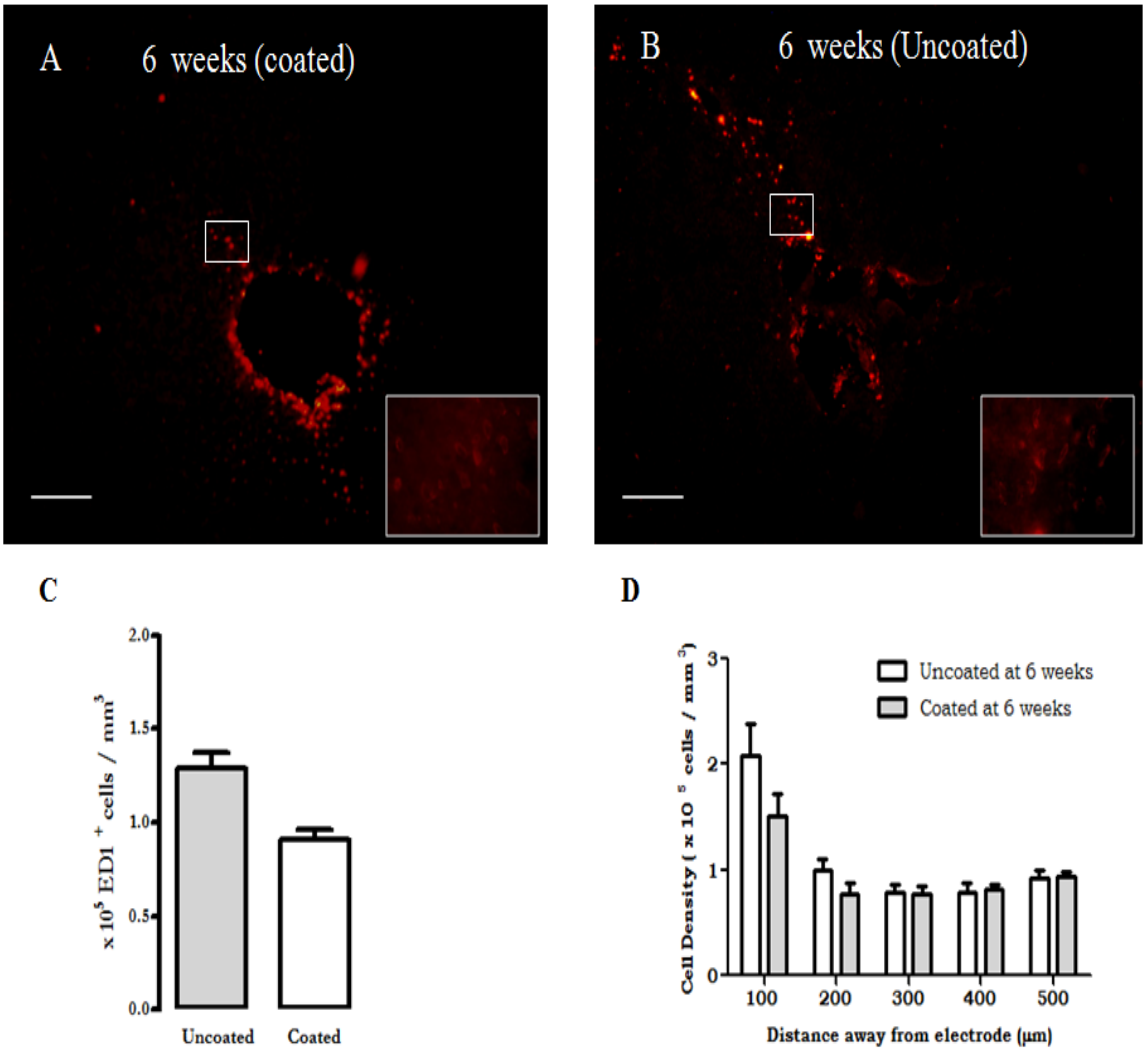

Figure 6. 4 : Quantitative cell density analysis of ED1 staining. (A) – (B) Representative images of ED1 staining for reactive microglia/ macrophages in the brain section 4 weeks post implantation for both coated and uncoated microelectrodes. Scale bar = 100 µm. (C) Estimation of overall ED1 cell density at 4 weeks post implantation. (D) $ED1^{+}$ cell density profile as a function of distance at 4 weeks post implantation. Statistical differences between uncoated and coated probes at the same time point are indicated by * ($p < 0.01$ comparing uncoated to the coated electrode)

6.3. GFAP immunoreactivity

6.3.1. Astrocyte Cell Density

The amount of astrocytic upregulation around the implant was characterized by GFAP staining. Stereologic analysis showed that there was an elevated astrocytic response near the uncoated electrode ($p < 0.001$, $F = 37.529$, $N = 500$). Additionally, the astrocytic response significantly varied at different distances away from electrode ($p < 0.001$, $F = 122.589$, $N= 500$). The overall data also illustrated that at different time points, there was a change in cell density ($p< 0.001$, $F = 17.883$, $N= 500$). Furthermore, the ANOVA showed an interaction between duration of implant and distance away electrode on overall cell density ($p < 0.001$, $F = 18.428$ $N= 500$), showing that cell density profile across distance changed over time.

At two weeks post implantation, the overall cell density around the coated implant was significantly lower than uncoated device (Figure 6.5-C). Both coated and control electrode sites had more GFAP positive cells near the electrode (0-100 μm) (Figure 6.5). At this time point, the difference in cell densities between coated and uncoated probes was significant up to 400 μm away from the injury site (Figure 6.5- D). GFAP staining revealed that astrocytes near the uncoated electrode became more proliferative, and elongated with thicker cellular processes. In both coated and uncoated devices, the cell distribution over the distance showed a similar pattern: heavy $GFAP^+$ cell density around the probe (1- 100 μm), and a drop of cell density after 100 μm region.

Four weeks after implantation, the coated electrode sites showed significantly lower overall cellular density, but the significance observed in the 0–100 μm domain at 2 weeks has been lost. The bulk of the disparity in coated vs. uncoated densities came from the 100-300 μm regions, where the coated electrode elicited less astrocytic response (Figure 6.6-D). Most astrocytes in this intensive area were proliferated compared with normal tissue away from the electrode. Also, the astrocyte processes were interwoven to form a dense meshwork. At 6 weeks after implantation, there was little difference in terms of $GFAP^+$ cell count between coated and uncoated electrode (Figure 6.7 – C). The overall immunostaining is lighter near the electrode for both coated and uncoated electrodes when compared to 2 and 4 week time points (Figure 6.7 – D).

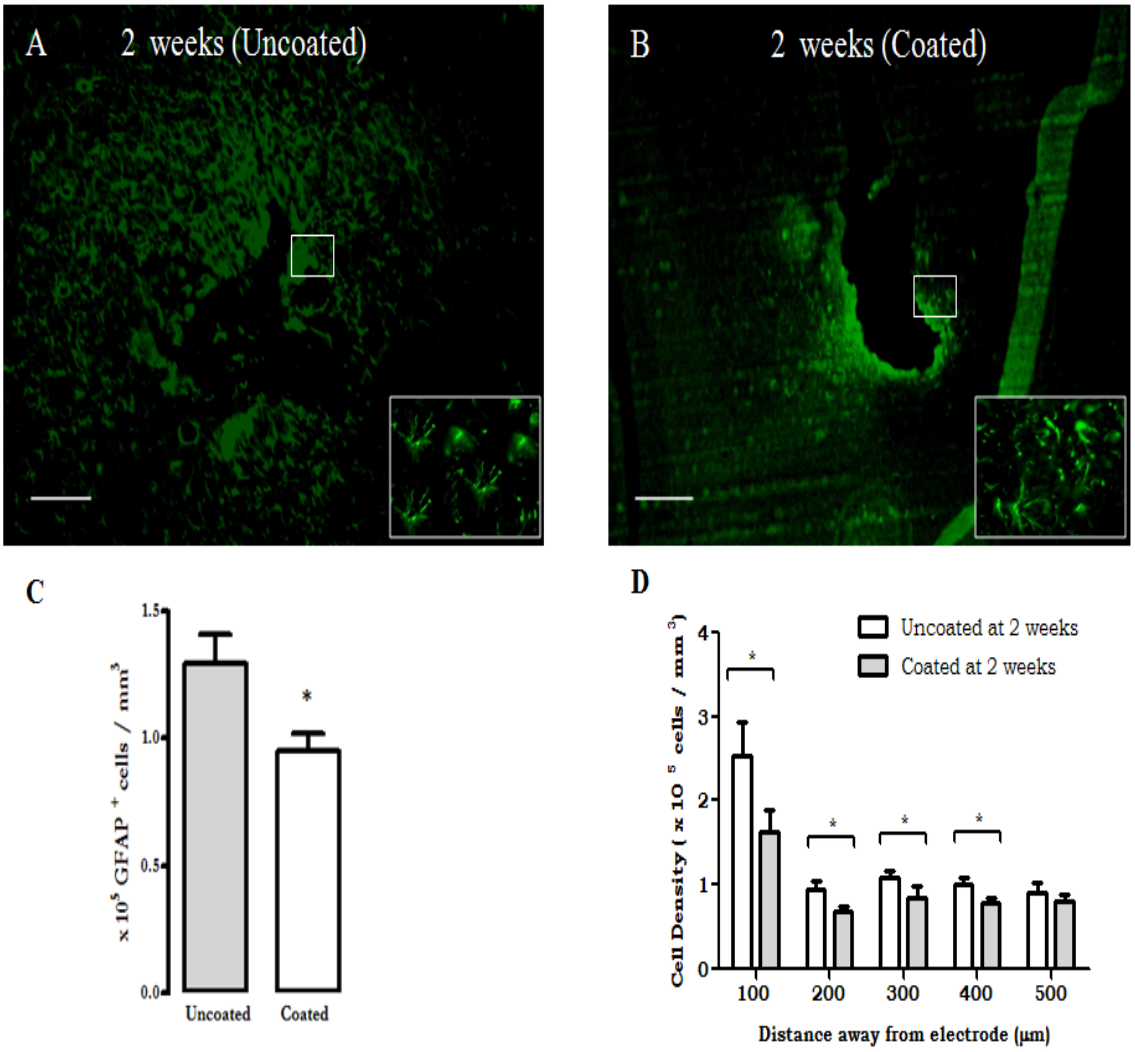

Figure 6. 5: Quantitative cell density analysis of GFAP staining. (A) – (B) Representative images of GFAP staining for reactive microglia/ macrophages in the brain section 2 weeks post implantation for both coated and uncoated microelectrodes. Scale bar = 100 µm. (C) Estimation of overall GFAP cell density at 2 weeks post implantation. (D) GFAP⁺ cell density profile as a function of distance at 2 weeks post implantation. Statistical differences between uncoated and coated probes at the same time point are indicated by * ($p < 0.01$ comparing uncoated to the coated electrode)

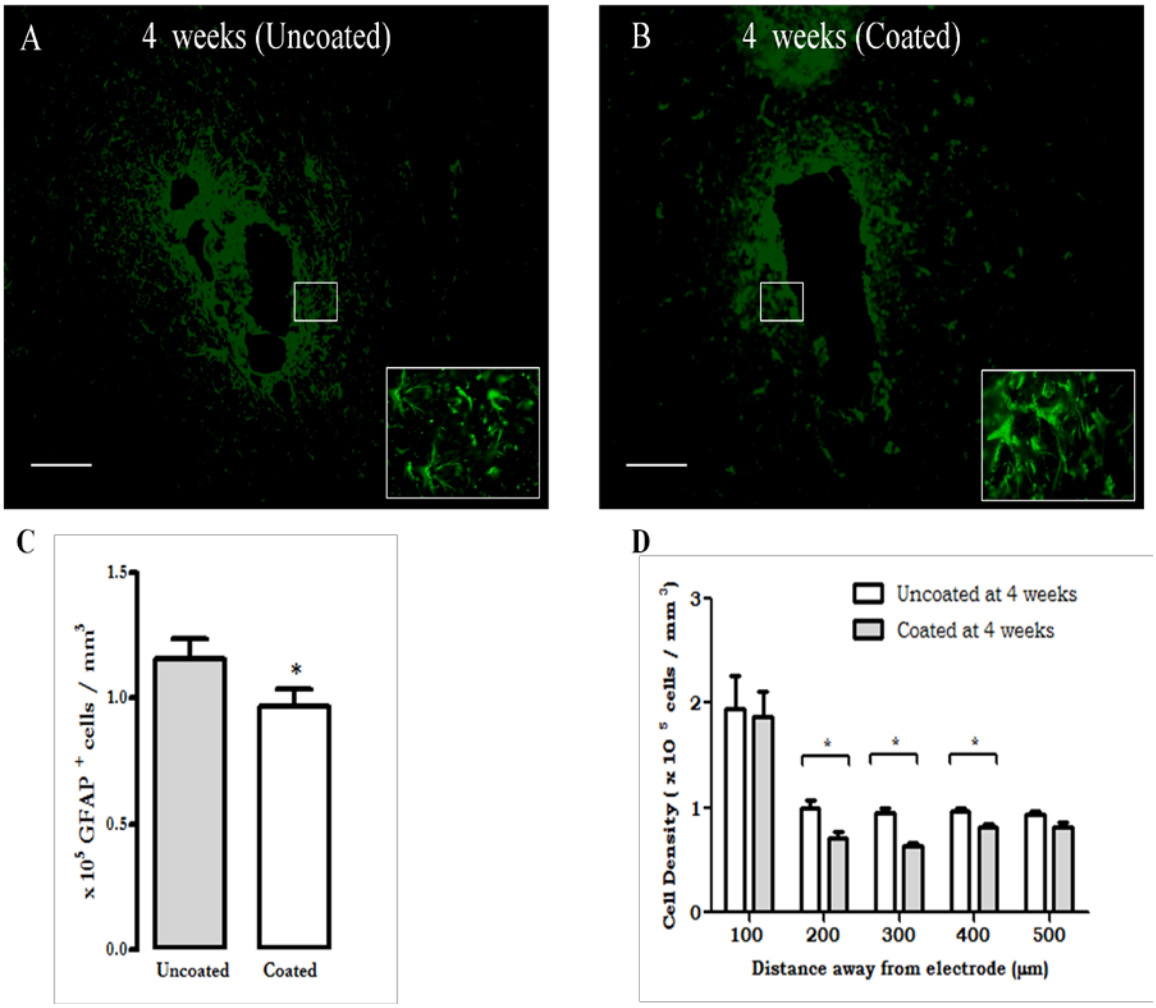

Figure 6.6 : Quantitative cell density analysis of GFAP staining. (A) – (B) Representative images of GFAP staining for reactive microglia/ macrophages in the brain section 4 weeks post implantation for both coated and uncoated microelectrodes. Scale bar = 100 µm. (C) Estimation of overall GFAP cell density at 4 weeks post implantation (D) $GFAP^+$ cell density profile as a function of distance at 2 weeks post implantation. Statistical differences between uncoated and coated probes at the same time point are indicated by * ($p < 0.01$ comparing uncoated to the coated electrode)

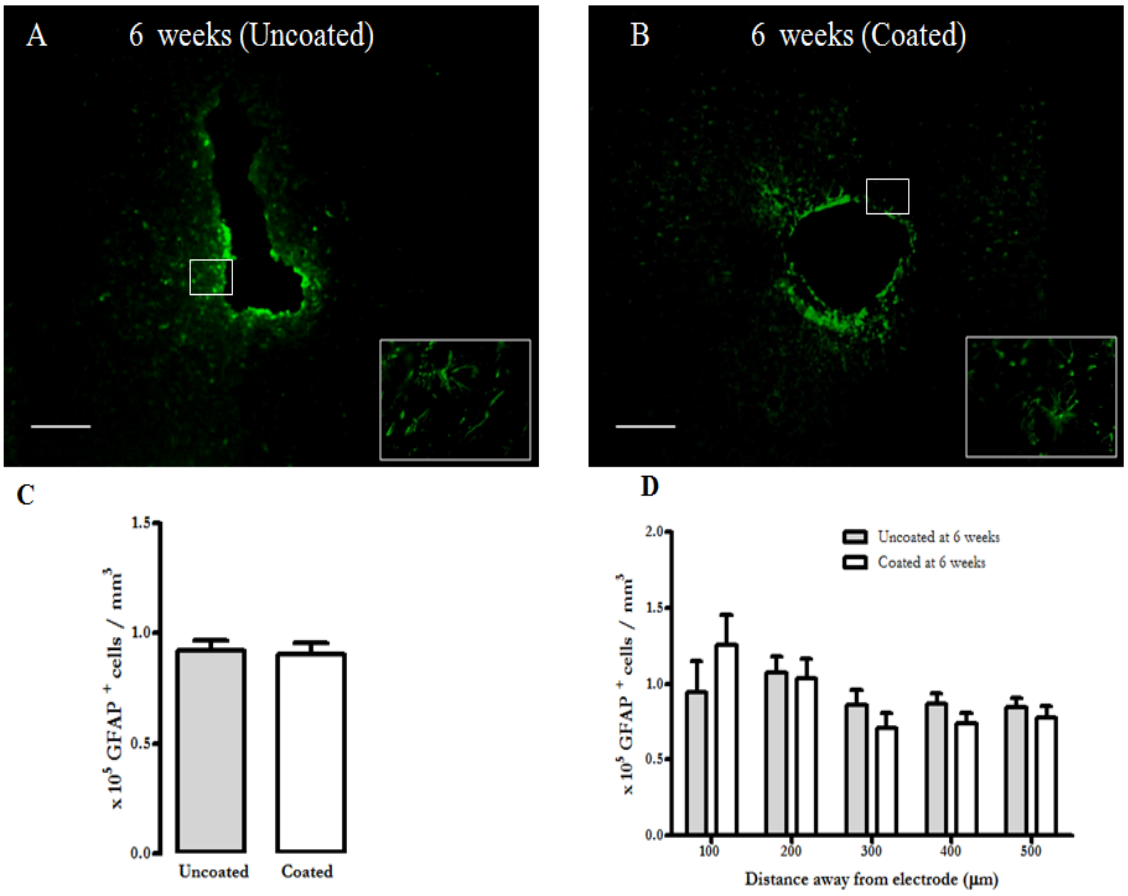

Figure 6.7: Quantitative cell density analysis of GFAP staining. (A) – (B) Representative images of GFAP staining for reactive microglia/ macrophages in the brain section 4 weeks post implantation for both coated and uncoated microelectrodes. Scale bar = 100 µm. (C) Estimation of overall GFAP cell density at 4 weeks post implantation (D) $GFAP^+$ cell density profile as a function of distance at 2 weeks post implantation. Statistical differences between uncoated and coated probes at the same time point are indicated by * ($P < 0.01$ comparing uncoated to the coated electrode)

6.3.2. GFAP intensity

In addition to $GFAP^+$ cell counts, a line intensity profile was implemented to assess the cellular hypertrophy near the electrode site. The GFAP staining intensity for the tissue adjacent to poloxamer coated device was consistently lower than staining adjacent to the uncoated device ($p < 0.001$, $F= 13.443$, $N = 384$). The ANOVA also showed a significant effect of: distance from electrode ($p < 0.001$, $F = 17.843$ $N= 384$), and duration of the implant ($p < 0.001$, $F = 119.858$ $N= 384$) on the GFAP intensity. For both coated and uncoated probes there was significantly higher intensity from the 0- 50 μm and declined thereafter.

At two weeks post insertion, there uncoated electrode was eliciting significantly more intense GFAP production than its PLX coated counterpart from 0-200um except for a small deviation from 50-100um, where $p = 0.015$ (Figure 6.7–A). Reactive astrocytes in the GFAP intensive area were hypertrophied and formed a dense network around the electrode. After 4 weeks, both control and uncoated electrodes exhibited increase in GFAP reactivity near the electrode (0- 50 μm). Even though the staining was consistently higher in the uncoated electrodes, the difference was not statistically significant at different domains (Figure 6.7-B). When compared to two weeks, the staining at 4 weeks was lower for both coated and uncoated probes, suggesting a decrease in astrocytic hypertrophy. Similar results were seen for GFAP intensity at 6 weeks, as there was an overall decrease in intensity level compared to two weeks. Additionally, there is no difference in the intensity profiles between coated and the

uncoated electrodes after six weeks (Figure 6.7-C). The lack of difference in staining around the coated electrode compared to the uncoated electrode suggests that the positive effect of poloxamer on altering up-regulation *in vivo* declined over time. This correlates with the cell count data, as astrocyte presence around the electrode were same after six weeks.

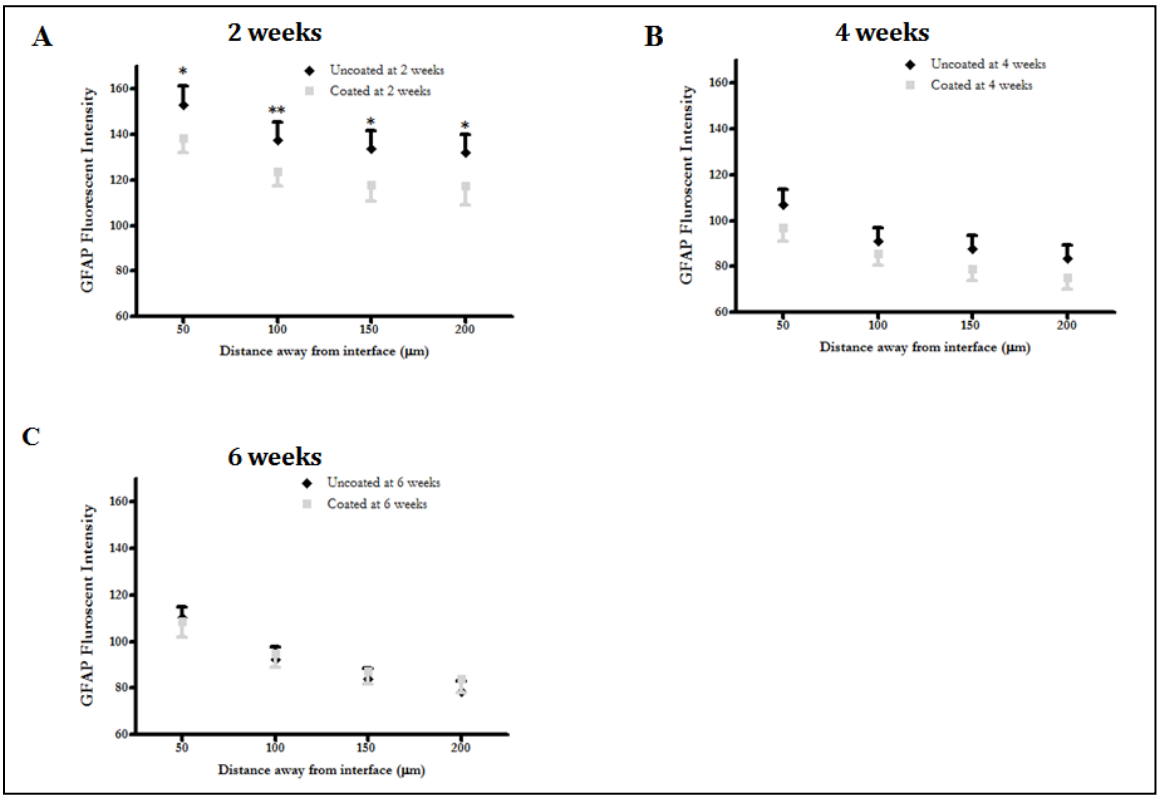

Figure 6.8: Quantitative fluorescent intensity analysis of GFAP staining. (A) GFAP fluorescent intensity profiles as a function of distance 2 weeks post implantation. (B) GFAP fluorescent intensity profiles as a function of distance 4 weeks post implantation. (C) GFAP$^+$ cell density profile as a function of distance at 2 weeks post implantation. (D) Estimation of overall GFAP cell density at 4 weeks post implantation. Statistical differences between uncoated and coated probes at the same time point are indicated by * ($p < 0.01$ comparing uncoated to the coated electrode) ** represents a p value approaching statistical significance ($p = 0.015$)

6.4. Presence of neurons around the electrode

Neuronal presence around the implanted electrode was characterized by counting $NeuN^+$ stained cells. NeuN staining is a standard marker for detecting neuronal nuclei. Our results indicate that, similar to ED-1 and GFAP staining, there was an effect of poloxamer on neuronal presence near the implant site ($p < 0.001$, $N = 530$, $F = 14.097$). The statistical model also showed a significant effect of: distance from electrode ($p < 0.001$, $F = 4.808$ $N= 530$) and duration of the implant ($p < 0.001$, $F = 6.270$ $N= 530$) on the neuronal density, suggesting that long term presence of the electrode causes a change in neuronal density near the electrode. At two weeks post implantation, pale NeuN staining was observed around in the area surrounding the electrode sites as compared to far field controls for both control and coated devices. The reduction in cell presence was most notable from 0-200um, beyond which the measures stabilized. Significantly higher numbers of neurons were counted near the coated electrode in all of bins, except in the region of 300–400 μm where the difference is approaching significance (Figure 6.8-A). Also, at the four week time point, the overall neuron density near the electrode was significantly higher, but surprisingly the difference between coated and uncoated at individual domains was not statistically significant (Figure 6.8–B). Similar results were seen after six weeks, as no statistical difference was seen between the two conditions (Figure 6.8-C). In summary, the overall neuronal cell density was significantly increased in PLX during the 2 week time point, but that significance was lost at 4 and 6 weeks. This suggests that in order for the

poloxamer to work over long period, we need to include a pharmacological agent such as nerve growth factor to support neuron growth beyond the glial scar.

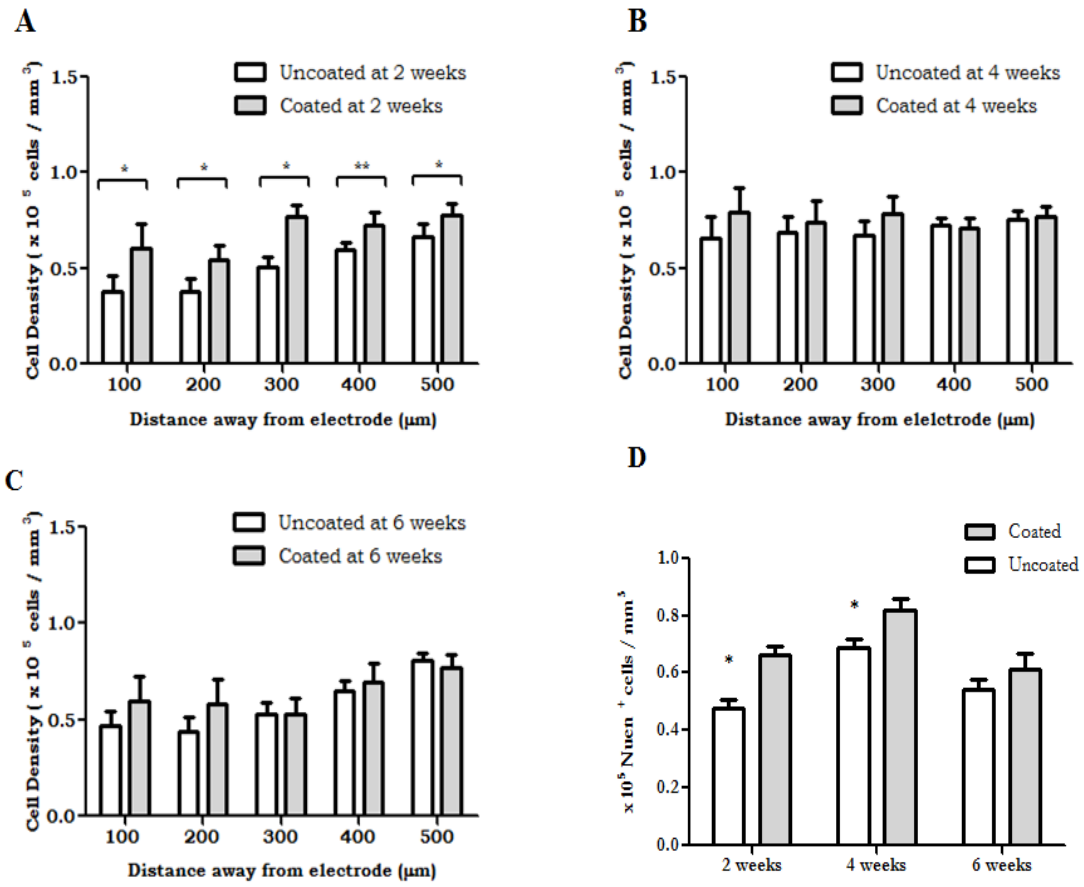

Figure 6. 9 : Quantitative Cell density of NeuN+ staining. (A)NeuN cell density profile as a function of distance 2 weeks post implantation. (B) NeuN+ cell density profiles as a function of distance 4 weeks post implantation. (C) $NeuN^{+}$ cell density profile as a function of distance at 6 weeks post implantation (D) Estimation of overall NeuN cell density at 2, 4, and 6 weeks post implantation. Statistical differences between uncoated and coated probes at the same time point are indicated by * ($p < 0.01$ comparing uncoated to the coated electrode) ** represents a p value approaching statistical significance ($p = 0.0130$)

7. DISCUSSION

The goal of this study was to assess the impact of the poloxamer coatings on *in vivo* brain tissue after implanting porous silicon structured ceramic microelectrodes. Previous studies have investigated the CNS response of poloxamer *in vitro* including neurons, and astrocytes [11, 57-58]. To the best of our knowledge, the effect of poloxamer on microglia/macrophage and astrocyte function *in vivo* has not been explored. This study uses the presence of neurons, macrophages /microglia, and reactive astrocytes to quantify the difference in *vivo* of coated and uncoated devices at 2, 4, and 6 weeks. In order to maintain long term single neuron recordings using ceramic microelectrodes, the environment around the recording area must promote neuronal survival and reduce inflammatory mediators that can confound measurements. This current study demonstrates that local release of poloxamer, a tri-block copolymer, via microelectrode coatings can modulate the acute inflammatory responses to implanted devices, especially by suppressing the expression of astrocytes and microglia while promoting neuronal survival.

The ability to record single neurons with implantable electrodes holds great promise for patients with impaired motor conditions caused by stroke, cervical spine injuries, and neurodegenerative diseases [14, 24, 62]. Among the various brain-computer interface (BCI) modalities, intracortical electrodes have several advantages for restoring voluntary motor control[3]. Using cortical microelectrodes, the sum of electrical activity around the electrode can be obtained by recording the electric potential in specific regions of the motor cortex. Near the electrode, the electric

potential is recorded by assessing the electrical fluctuations due to changes in membrane potential of neurons[63]. Thus, it is important to have neurons near the electrode (within 100 μm) in order for the electrode to record these signals. However, the insertion of a microelectrode reduces the neuron population near the device and causes a decrease in the amplitude of the action potential making it hard to discriminate the signal from background activity[63]. Additionally, the electrode insertion induces an astroglial scar which keeps neurons away from the recording device. Currently, multiple approaches are being investigated in order to reduce tissue response and improving long-term device utilization.

Following an implantation induced injury, host neurons in CNS cannot be repaired due to the inability of the neurons to regenerate [14]. This is primarily due to the presence of inhibitory glycoproteins in the environment, which eventually lead to reactive gliosis. The primary cell types involved in this glial scar formation are microglia/ macrophages and astrocytes[24]. The surgical insertion of the microelectrode will inevitably damage neurons, tearing dendritic and axonal processes and potentially inducing some neuronal cell death [17]. As a result of the vascular damage and release of chemotatic factors caused by electrode, circulating monocytes and microglia from brain tissue migrate to the injury site and become activated [53]. One typical indication of an activated microglial cells is their transformation into macrophage like amoeboid cell structures [64-65]. In our study, *in vivo* microglial/ macrophage cell density was assessed next to the insertion site at various time points. The $ED1^{+}$ cell density decreases significantly as a function of distance away from the electrode, suggestive of a microglial upregulation, which moves to wall off the foreign

implanted electrode. This decrease in microglia/ macrophage response was significantly attenuated in PLX coated probes when compared and uncoated ones after 2 weeks, and 4 weeks post implantation. Although, no statistical difference was observed after six weeks, the uncoated electrode induced a considerably higher glial activation at this time point. Our results of microglial modulation by poloxamer coatings are similar to observations made by Zhong et al [12]. In their study, dexamethasone (DEX) coatings significantly reduced microglial activation initially, however no significant difference in ED1 staining was observed between the uncoated and coated after four weeks of implantation. Previously, studies have shown that initially microglia release various cytokines which attract adjacent microglia and astrocytes to the injury site, via autocrine and paracrine pathways leading to recruitment of glial cells [66]. Our results indicate that poloxamer has an initial inhibitory effect on microglial response supported by lower ED-1 response for coated devices at 2 and 4 weeks. One possible explanation for the modulation of this response at earlier time points is that poloxamer self inserts into the damaged cell membranes and reduces the amount of debris, thus limiting the buildup of phagocytic microglia and macrophages. However, at after 6 weeks, the lack of significant difference between the coated and uncoated conditions could be due to depletion of the polymer, or the stabilization of the microglial response. After a long period *in vivo*, depletion of the poloxamer is highly likely because the coating was applied via dipping method. The initial loading and diffusion of poloxamer *in vivo* must be examined in detail to establish this as a causative factor for the loss of its effect by 6 weeks.

In addition to microglia and macrophages, astrocytes also participate in the glial scar formation following an electrode implantation. After injury, astrocytes near the injury site become reactive and secrete neural growth factor (NGF), which helps in repairing neural tissue [36]. The reactive astrocytes exhibit phenotypic changes characterized by hypertrophy and increase in expression of glial fibrillary acidic protein (GFAP), which is critical to astrocyte function and their ability to support neighboring damaged neurons.[24]. In our approach, we assessed the degree of recruitment (cell count) and degree of cellular activity (GFAP stain intensity). Stereological analysis has shown that there was a relative buildup of reactive astrocytes within 100 μm of both coated and uncoated electrode sites as compared to far field controls. These reactive astrocytes are characterized by higher GFAP expression and formation of dense processes near the injury site. The formation of an astrocytic barrier, separating the injury site from healthy tissue was previously shown in multiple studies [9, 13]. In PLX coated electrodes, the decrease in astrocytic response was similar to that of the microglia/macrophage response. This response shows the crosstalk between microglia and astrocytes during glial scar formation [67-68]. Both microglia and astrocytes have the capability of releasing neurotoxic cytokines, which can activate more astrocytes or microglia via paracrine and autocrine signaling [65-66]. At 2 and 4 weeks, poloxamer helped minimize astrocyte buildup, attesting the capability of this surfactant to limit damage and enable fast repair of the brain tissue.

In our efforts to quantify cellular hypertrophy, we implanted a line intensity analysis as described in previous studies [13, 20]. Our results showed a similar pattern to cell density. The ANOVA model showed significant effect of distance and duration of

implant on staining intensity. Similar to other studies reported in past, higher levels of GFAP expression were seen closest to the insertion sites (0-50 μm) of both coated and uncoated devices [12]. As with our other measures, the PLX showed a significant decrease in GFAP intensity at both 2 and 4 weeks.

After 6 weeks post-implantation, the astrocyte sheath around both uncoated and coated probes had lower intensity and yielded no significant difference between the two conditions. The significant reduction of reactive astrocytes suggests that the inflammatory response starts to stabilize at 6 week in our animal model. These results are consistent with other studies, where it was reported that the astrocytic sheath around the injury site grows in size for several weeks, after which the encapsulation layer becomes thinner, denser and stabilizes after approximately six weeks [9]. Given the loss of significance by 6 weeks, two distinct possibilities emerge as to why. First, the loading of poloxamer may have been insufficient and the loading dose had diffused/decayed to sub-therapeutic levels. Second, the approach may be more suited to reducing initial injury related inflammation than the more prolonged foreign body response

Lastly, neuronal presence around the electrodes was quantified near the implant site. There was a negative correlation between glial cell types and neurons, suggesting that increase in glia pushes the neurons away from the microelectrode. This may be attributed to the fact that in the in activated state, microglia and astrocytes secrete toxic materials including cytokines, nitric oxide (NO), and free radical species which contribute to neuronal loss [32, 66]. At two weeks, the neuron cell population was markedly lower near the electrode and stabilized in the far field, however at 4 and 6

weeks there was no variation in cell density as a function of distance from the implant. NeuN staining revealed that PLX coating has reduced the neuronal loss at 2 and 4 weeks after implantation.

This attests the nature of poloxamer, which was shown to act as a neuroprotective agent. When neurons are exposed to injury, damage to membranes can lead to either necrosis or apoptosis [11, 57]. In an *in vitro* cell model, it was shown that PLX has the ability to prevent acute necrosis by promoting membrane resealing and additionally PLX treatment inhibits signaling pathways leading to apoptosis [11, 57]. By 6 weeks, there was no difference between PLX coated and uncoated probes in terms of neuronal loss. Interestingly, at 6 weeks the neuronal loss increased as compared to 4 weeks. This was consistent with lower microglia/ macrophage activation and astrocyte expression at 6 weeks. Similar results were shown in studies conducted by Zhong *et al* [12]. One possible explanation is that over time, the stabilized immune response induces a buildup of secreted neurotoxic molecules which leads to progressive neuronal loss. Thus, inhibiting the glial activation via poloxamer coatings can enhance neuronal survival and ultimately support long term recordings.

Long term implantation of microelectrodes in the brain induces two major responses. First, insertion of electrode through the cortex causes mechanical damage to neuronal and glial processes, exposing the extracellular environment to intracellular proteins and damaging the blood-brain barrier [17]. Secondly, continued presence of the electrode induces the release of toxic molecules and leads to a glial scar which walls off the microelectrode from recording single neurons [17]. The initial mechanical damage and long term foreign body interact in a complex manner to cause the loss of

neuronal recordings. Processes initiated during the early phase of the glial scar persist and contribute to eventual encapsulation of the electrode [17]. Our previous study has reported that one way to ameliorate damage to neurons is by mimicking the surface of the electrode to that of the brain [17, 41]. Nanostructured porous silicon surface coatings for ceramic-based microelectrodes showed less glial activation and more neurons adjacent to porous silicon surfaces than smooth silicon surfaces [17]. In this current study, we use a local drug delivery approach to further improve the nanostructured porous silicon devices by coating with poloxamer – 188, a neuro-protective agent, in order to reduce cellular and molecular inflammatory responses to the implanted microelectrodes. While positive results were found in response at 2 and 4 weeks, after 6 weeks, poloxamer had no positive effect due to possible drug depletion and stabilization of inflammatory cells around the implantation site. Thus, in order to obtain long-term stable neural recordings we must discover the release profile of poloxamer *in vivo.* Further improvements can be made to release profile by encapsulating in a biodegradable polymer. An alternative strategy could be to develop a drug delivery system that facilitates continuous, local delivery of the poloxamer for the long periods of time. A recent study conducted by Abidian *et al.* described a similar approach [69]. In this study, controlled release was achieved in silicon electrodes *in vitro* using a coating of polymer matrix loaded with the dexamethasone, a synthetic glucocorticoid [69]. Even though these devices have not yet been tested *in vivo,* the promising results highlight the potential of electrode coatings in improving chronic neuroprosthetic performance.

In conclusion, the surface modification of nanostructured porous silicon ceramic electrodes with poloxamer coating is able to reduce the tissue response near the implants. The local delivery of PLX might be a promising strategy to improve the long term recording stability of multichannel ceramic microelectrodes.

8. CONCLUSION

This study assessed the neuroprotective effects of poloxamer coatings *in vivo*. Ceramic electrodes with and without PLX coatings were implanted into rats, and the tissue response was evaluated 2 weeks, 4 weeks, and 6 weeks post implantation. Our results indicate that PLX coatings significantly reduced microglia/ macrophage expression at two weeks and four weeks implantation. Similarly, glial fibrillary acidic protein (GFAP) staining for reactive astrocytes revealed that local PLX treatment significantly modulated astroglial cell density and cell hypertrophy near the electrode at 2 and 4 weeks. A reciprocal relationship was seen with neuronal presence around the implant site. The PLX coating decreased neuronal loss at 2, and 4 weeks after implantation. However weak ED1, GFAP, and NEUN positive signal was detected after 6 weeks post implantation for the coated devices, suggesting that coating is not enough to modulate chronic inflammatory response. However, lower microglial presence was seen at 6 weeks even though this difference was significant. Thus, it is important to do future long term studies to determine if delivery of PLX in early stage is sufficient for mitigating the tissue response. Another strategy will be to implement a continuous drug system that will release PLX throughout the lifetime of the electrode. In summary, this study demonstrated that PLX coatings can effectively modulate the inflammatory cell response to the implanted microelectrodes, and also reduce neuronal loss in the vicinity of the coated devices after four weeks. This strategy represents a promoting way to reduce astroglial scar

and prevent neuronal loss after microelectrode implantation, ultimately leading to long term neuron recordings.

9. FUTURE WORK

Release profile of PLX *in vivo*

Previous work in our lab studied the release of PLX *in vitro*; however the *in vivo* release profile must also be understood. This could be done using a radiolabel PLX, which can used to quantify the *in vivo* release over time. A study can be developed where radio labeled PLX coated electrodes will be implanted at different time points and the distribution of the PLX will be observed using autoradiography. For quantification of radio labeled PLX, horizontal sections will cut using cryostat and used for autoradiography. These results can be correlated with results from histological analysis and a model can be developed to optimize initial loading of the poloxamer.

Chronic Neural Recordings

The long term goal of this research is to achieve chronic single neuron recordings from ceramic electrodes. In order to do this, the inflammatory response around the devices must be minimized. This study showed significant decrease of inflammatory responses and neuronal loss around the PLX coated electrodes. However, it is important to correlate this improvement in tissue response to the long-term recording performance of the ceramic microelectrodes. The loss of recordings *in vivo* can be attributed to two factors: the migration of neurons away from the electrode and increase of the electrode impedance. The impedance change

will result to too much noise and lead to inconsistent recordings whereas the isolation of neurons leads to low signal-to-noise ratio (SNR) or unresolvable action potentials (noise). In order to examine the potential of PLX coatings, a study can developed to test parameters such as single unit stability, signal-to-noise ratio, recording longevity, and electrode impedance. The histology results then can be correlated with these parameters to evaluate the effect of coatings on electrode performance.

Neurotrophic Factor delivery for neuronal survival

One of the main reasons for the failure of chronic recordings is due to the migration of neurons away from the electrode. This study demonstrated that PLX decreased neuronal loss around the electrode. However it is not known whether this improved is sufficient to ensure chronic recordings. If PLX is not able to keep neurons close to the electrode sites after long periods, one strategy to attract neurons near the electrode is by delivering Brain derived neurotrophic factor (BDNF). BDNF is shown to promote neuronal survival in the CNS. Studies have reported that after spinal cord injury, BDNF stimulated neurite growth and allowed functional recovery [70-71]. Therefore applying BDNF to the PLX coated electrodes is an excellent way to promote neuronal survival and migration to the electrode site. Previous work in the lab has used BDNF coatings to ceramic electrodes, however their effect is not observed along with PLX.

10. REFERENCES

[1] J. P. Donoghue, "Connecting cortex to machines: recent advances in brain interfaces," *Nat Neurosci,* vol. 5 Suppl, pp. 1085-8, Nov 2002.

[2] J. C. Sanchez*, et al.*, "Ascertaining the importance of neurons to develop better brain-machine interfaces," *Ieee Transactions on Biomedical Engineering,* vol. 51, pp. 943-953, Jun 2004.

[3] L. R. Hochberg and J. P. Donoghue, "Sensors for brain-computer interfaces," *IEEE Eng Med Biol Mag,* vol. 25, pp. 32-8, Sep-Oct 2006.

[4] L. R. Hochberg*, et al.*, "Neuronal ensemble control of prosthetic devices by a human with tetraplegia," *Nature,* vol. 442, pp. 164-71, Jul 13 2006.

[5] K. A. Moxon*, et al.*, "Ceramic-based multisite electrode arrays for chronic single-neuron recording," *IEEE Trans Biomed Eng,* vol. 51, pp. 647-56, Apr 2004.

[6] W. M. Grill*, et al.*, "Implanted neural interfaces: biochallenges and engineered solutions," *Annu Rev Biomed Eng,* vol. 11, pp. 1-24, 2009.

[7] D. R. Kipke*, et al.*, "Silicon-substrate intracortical microelectrode arrays for long-term recording of neuronal spike activity in cerebral cortex," *IEEE Trans Neural Syst Rehabil Eng,* vol. 11, pp. 151-5, Jun 2003.

[8] V. S. Polikov*, et al.*, "Response of brain tissue to chronically implanted neural electrodes," *J Neurosci Methods,* vol. 148, pp. 1-18, Oct 15 2005.

[9] D. H. Szarowski*, et al.*, "Brain responses to micro-machined silicon devices," *Brain Res,* vol. 983, pp. 23-35, Sep 5 2003.

[10] R. J. Vetter*, et al.*, "Chronic neural recording using silicon-substrate microelectrode arrays implanted in cerebral cortex," *IEEE Trans Biomed Eng,* vol. 51, pp. 896-904, Jun 2004.

[11] G. Serbest*, et al.*, "The effect of Poloxamer-188 on neuronal cell recovery from mechanical injury," *Journal of Neurotrauma,* vol. 22, pp. 119-132, Jan 2005.

[12] Y. Zhong and R. V. Bellamkonda, "Dexamethasone-coated neural probes elicit attenuated inflammatory response and neuronal loss compared to uncoated neural probes," *Brain Res,* vol. 1148, pp. 15-27, May 7 2007.

[13] W. He*, et al.*, "Nanoscale laminin coating modulates cortical scarring response around implanted silicon microelectrode arrays," *J Neural Eng,* vol. 3, pp. 316-26, Dec 2006.

[14] A. B. Schwartz, "Cortical neural prosthetics," *Annu Rev Neurosci,* vol. 27, pp. 487-507, 2004.

[15] C. E. Schmidt and J. B. Leach, "Neural tissue engineering: strategies for repair and regeneration," *Annu Rev Biomed Eng,* vol. 5, pp. 293-347, 2003.

[16] J. Stroncek and W. M. Reichert, "Overview of Wound Healing in Different Tissue Types," in *Indwelling Neural Implants: Strategies for Contending with the In Vivo Environment*, ed Boca Raton: CRC Press, 2008.

[17] K. A. Moxon*, et al.*, "Bioactive properties of nanostructured porous silicon for enhancing electrode to neuron interfaces," *J Biomater Sci Polym Ed,* vol. 18, pp. 1263-81, 2007.

[18] J. M. Anderson*, et al.*, "Foreign body reaction to biomaterials," *Semin Immunol,* vol. 20, pp. 86-100, Apr 2008.

[19] D. J. Edell*, et al.*, "Factors influencing the biocompatibility of insertable silicon microshafts in cerebral cortex," *IEEE Trans Biomed Eng,* vol. 39, pp. 635-43, Jun 1992.

[20] R. Biran*, et al.*, "Neuronal cell loss accompanies the brain tissue response to chronically implanted silicon microelectrode arrays," *Exp Neurol,* vol. 195, pp. 115-26, Sep 2005.

[21] X. Liu*, et al.*, "Stability of the interface between neural tissue and chronically implanted intracortical microelectrodes," *IEEE Trans Rehabil Eng,* vol. 7, pp. 315-26, Sep 1999.

[22] R. W. Griffith and D. R. Humphrey, "Long-term gliosis around chronically implanted platinum electrodes in the Rhesus macaque motor cortex," *Neurosci Lett,* vol. 406, pp. 81-6, Oct 2 2006.

[23] J. P. Seymour and D. R. Kipke, "Neural probe design for reduced tissue encapsulation in CNS," *Biomaterials,* vol. 28, pp. 3594-607, Sep 2007.

[24] Y. Zhong and R. V. Bellamkonda, "Biomaterials for the central nervous system," *J R Soc Interface,* vol. 5, pp. 957-75, Sep 6 2008.

[25] W. He and R. V. Bellamkonda, "A molecular perspective on understanding and modulating the performance of chronic cns recording electrodes," in *Indwelling Neural Implants: Strategies for Contending with the In Vivo Environment*, ed Boca Raton: CRC Press, 2008.

[26] E. A. Ling and W. C. Wong, "The origin and nature of ramified and amoeboid microglia: a historical review and current concepts," *Glia,* vol. 7, pp. 9-18, Jan 1993.

[27] G. Raivich*, et al.*, "Regulation of MCSF receptors on microglia in the normal and injured mouse central nervous system: a quantitative immunofluorescence study using confocal laser microscopy," *J Comp Neurol,* vol. 395, pp. 342-58, Jun 8 1998.

[28] L. Minghetti*, et al.*, "Microglial activation in chronic neurodegenerative diseases: roles of apoptotic neurons and chronic stimulation," *Brain Res Brain Res Rev,* vol. 48, pp. 251-6, Apr 2005.

[29] C. Wiesmann and A. M. de Vos, "Nerve growth factor: structure and function," *Cell Mol Life Sci,* vol. 58, pp. 748-59, May 2001.

[30] K. Moore*, et al.*, "Immobilized concentration gradients of neurotrophic factors guide neurite outgrowth of primary neurons in macroporous scaffolds," *Tissue Eng,* vol. 12, pp. 267-78, Feb 2006.

[31] A. A. Babcock*, et al.*, "Chemokine expression by glial cells directs leukocytes to sites of axonal injury in the CNS," *J Neurosci,* vol. 23, pp. 7922-30, Aug 27 2003.

[32] M. T. Fitch*, et al.*, "Cellular and molecular mechanisms of glial scarring and progressive cavitation: in vivo and in vitro analysis of inflammation-induced secondary injury after CNS trauma," *J Neurosci,* vol. 19, pp. 8182-98, Oct 1 1999.

[33] A. K. McNally and J. M. Anderson, "Beta1 and beta2 integrins mediate adhesion during macrophage fusion and multinucleated foreign body giant cell formation," *Am J Pathol,* vol. 160, pp. 621-30, Feb 2002.

[34] K. Nakajima*, et al.*, "Neurotrophin secretion from cultured microglia," *J Neurosci Res,* vol. 65, pp. 322-31, Aug 15 2001.

[35] C. L. Klaver and M. R. Caplan, "Bioactive surface for neural electrodes: decreasing astrocyte proliferation via transforming growth factor-beta1," *J Biomed Mater Res A,* vol. 81, pp. 1011-6, Jun 15 2007.

[36] J. R. Goss*, et al.*, "Astrocytes are the major source of nerve growth factor upregulation following traumatic brain injury in the rat," *Exp Neurol,* vol. 149, pp. 301-9, Feb 1998.

[37] J. N. Turner*, et al.*, "Cerebral astrocyte response to micromachined silicon implants," *Exp Neurol,* vol. 156, pp. 33-49, Mar 1999.

[38] K. Moxon*, et al.*, "Long-Term Recordings of Multiple, Single-Neurons for Clinical Applications: The Emerging Role of the Bioactive Microelectrode," *Materials,* vol. 2, pp. 1762-1794, 2009.

[39] P. J. Rousche*, et al.*, "Flexible polyimide-based intracortical electrode arrays with bioactive capability," *IEEE Trans Biomed Eng,* vol. 48, pp. 361-71, Mar 2001.

[40] A. Singh*, et al.*, "Glial cell and fibroblast cytotoxicity study on plasma-deposited diamond-like carbon coatings," *Biomaterials,* vol. 24, pp. 5083-9, Dec 2003.

[41] K. A. Moxon*, et al.*, "Nanostructured surface modification of ceramic-based microelectrodes to enhance biocompatibility for a direct brain-machine interface," *IEEE Trans Biomed Eng,* vol. 51, pp. 881-9, Jun 2004.

[42] Y. Xiao, *et al.*, "Surface modification of neural probes with conducting polymer poly(hydroxymethylated-3,4- ethylenedioxythiophene) and its biocompatibility," *Appl Biochem Biotechnol,* vol. 128, pp. 117-30, Feb 2006.

[43] X. Cui, *et al.*, "Surface modification of neural recording electrodes with conducting polymer/biomolecule blends," *Journal of Biomedical Materials Research,* vol. 56, pp. 261-72, Aug 2001.

[44] S. T. Retterer, *et al.*, "Model neural prostheses with integrated microfluidics: a potential intervention strategy for controlling reactive cell and tissue responses," *IEEE Trans Biomed Eng,* vol. 51, pp. 2063-73, Nov 2004.

[45] S. T. Retterer, *et al.*, "Constant pressure fluid infusion into rat neocortex from implantable microfluidic devices," *J Neural Eng,* vol. 5, pp. 385-91, Dec 2008.

[46] K. C. Cheung, "Implantable microscale neural interfaces," *Biomed Microdevices,* vol. 9, pp. 923-38, Dec 2007.

[47] Y. Koyama, *et al.*, "BQ788, an endothelin ET(B) receptor antagonist, attenuates stab wound injury-induced reactive astrocytes in rat brain," *Glia,* vol. 26, pp. 268-71, May 1999.

[48] W. S. Sheng, *et al.*, "Tumor necrosis factor alpha upregulates human microglial cell production of interleukin-10 in vitro," *Clin Diagn Lab Immunol,* vol. 2, pp. 604-8, Sep 1995.

[49] Y. I. Tomobe, *et al.*, "Anticoagulant factor protein S inhibits the proliferation of rat astrocytes after injury," *Neurosci Lett,* vol. 214, pp. 57-60, Aug 16 1996.

[50] L. Spataro, *et al.*, "Dexamethasone treatment reduces astroglia responses to inserted neuroprosthetic devices in rat neocortex," *Exp Neurol,* vol. 194, pp. 289-300, Aug 2005.

[51] W. Shain, *et al.*, "Controlling cellular reactive responses around neural prosthetic devices using peripheral and local intervention strategies," *IEEE Trans Neural Syst Rehabil Eng,* vol. 11, pp. 186-8, Jun 2003.

[52] D. H. Kim and D. C. Martin, "Sustained release of dexamethasone from hydrophilic matrices using PLGA nanoparticles for neural drug delivery," *Biomaterials,* vol. 27, pp. 3031-7, May 2006.

[53] C. S. Bjornsson, *et al.*, "Effects of insertion conditions on tissue strain and vascular damage during neuroprosthetic device insertion," *J Neural Eng,* vol. 3, pp. 196-207, Sep 2006.

[54] R. Wadhwa, *et al.*, "Electrochemically controlled release of dexamethasone from conducting polymer polypyrrole coated electrode," *J Control Release,* vol. 110, pp. 531-41, Feb 21 2006.

[55] J. D. Marks, *et al.*, "Amphiphilic, tri-block copolymers provide potent membrane-targeted neuroprotection," *FASEB J,* vol. 15, pp. 1107-9, Apr 2001.

[56] S. A. Maskarinec, *et al.*, "Direct observation of poloxamer 188 insertion into lipid monolayers," *Biophys J,* vol. 82, pp. 1453-9, Mar 2002.

[57] G. Serbest, *et al.*, "Mechanisms of cell death and neuroprotection by poloxamer 188 after mechanical trauma," *FASEB J,* vol. 20, pp. 308-10, Feb 2006.

[58] D. Kilinc, *et al.*, "Poloxamer 188 reduces axonal beading following mechanical trauma to cultured neurons," *Conf Proc IEEE Eng Med Biol Soc,* vol. 2007, pp. 5395-8, 2007.

[59] B. K. Leung, *et al.*, "Characterization of microglial attachment and cytokine release on biomaterials of differing surface chemistry," *Biomaterials,* vol. 29, pp. 3289-97, Aug 2008.

[60] J. Nissanov, *et al.*, "Cryosectioning distortion reduction using tape support," *Microsc Res Tech,* vol. 53, pp. 239-40, May 1 2001.

[61] M. J. West, "Design-based stereological methods for counting neurons," *Prog Brain Res,* vol. 135, pp. 43-51, 2002.

[62] S. Breit, *et al.*, "Deep brain stimulation," *Cell Tissue Res,* vol. 318, pp. 275-88, Oct 2004.

[63] M. D. Johnson, *et al.*, "Repeated voltage biasing improves unit recordings by reducing resistive tissue impedances," *IEEE Trans Neural Syst Rehabil Eng,* vol. 13, pp. 160-5, Jun 2005.

[64] J. W. Fawcett and R. A. Asher, "The glial scar and central nervous system repair," *Brain Res Bull,* vol. 49, pp. 377-91, Aug 1999.

[65] G. W. Kreutzberg, "Microglia: a sensor for pathological events in the CNS," *Trends Neurosci,* vol. 19, pp. 312-8, Aug 1996.

[66] A. Takeuchi, *et al.*, "Macrophage colony-stimulating factor is expressed in neuron and microglia after focal brain injury," *J Neurosci Res,* vol. 65, pp. 38-44, Jul 1 2001.

[67] U. K. Hanisch and H. Kettenmann, "Microglia: active sensor and versatile effector cells in the normal and pathologic brain," *Nat Neurosci,* vol. 10, pp. 1387-94, Nov 2007.

[68] U. K. Hanisch, "Microglia as a source and target of cytokines," *Glia,* vol. 40, pp. 140-55, Nov 2002.

[69] M. R. Abidian, *et al.*, "Interfacing Conducting Polymer Nanotubes with the Central Nervous System: Chronic Neural Recording using Poly (3,4-ethylenedioxythiophene) Nanotubes," *Advanced Materials,* vol. 21, pp. 3764-3770, Oct 5 2009.

[70] C. A. Tobias*, et al.*, "Alginate encapsulated BDNF-producing fibroblast grafts permit recovery of function after spinal cord injury in the absence of immune suppression," *J Neurotrauma,* vol. 22, pp. 138-56, Jan 2005.

[71] A. Jain*, et al.*, "In situ gelling hydrogels for conformal repair of spinal cord defects, and local delivery of BDNF after spinal cord injury," *Biomaterials,* vol. 27, pp. 497-504, Jan 2006.